Resonant Scattering Manipulation of Dielectric Nanoparticles

Jiahui Xu, Yue Wu, Pinzheng Zhang, Yiming Wu, Renaud a L Vallée, Suli Wu, Xiaogang Liu

DOI: /((please add manuscript number))
Article type: Review

Resonant Scattering Manipulation of Dielectric Nanoparticles

Jiahui Xu, Yue Wu, Pinzheng Zhang, Yiming Wu, Renaud A. L. Vallée, Suli Wu and Xiaogang Liu**

Dr. J. Xu, P. Zhang, Dr. Y. Wu, Prof. X. Liu
Department of Chemistry and The N.1 Institute for Health, National University of Singapore, Singapore 117543, Singapore
E-mail: chmlx@nus.edu.sg

Y. Wu, Prof. S.Wu
State Key Laboratory of Fine Chemicals, Dalian University of Technology, Dalian 116024, China.
E-mail: wusuli@dlut.edu.cn

Dr. R. A. L. Vallée
CNRS, University of Bordeaux, CRPP-UMR 5031, Pessac 33600, France

Keywords: Dielectric nanoparticles, Mie scattering, electromagnetic resonance, all-dielectric nanostructures, magnetic light

Abstract: The concentration and manipulation of light in the nanoscale range are fundamental to nanophotonic research. Plasmonic nanoparticles can localize electromagnetic waves within subdiffraction volumes, but they also undergo large Joule losses and inevitable thermal heating. Subwavelength dielectric nanoparticles have emerged as a new class of photonic building blocks that enhance light-matter interactions within nanometric volumes. These nanoparticles exhibit strong electric and magnetic responses with negligible energy dissipation. In recent decades, the design of efficient dielectric nanoresonators has seen tremendous progress. In this review, we discuss recent theoretical and experimental advances in characterizing the optical properties of dielectric nanoparticles, from resonant single-particle scattering characteristics to multimodal interference in complex particle assemblies. Specific attention is paid to novel strategies employed to manipulate far-field Mie-type scattering, enhance local electromagnetic field, and boost magnetic resonance, as well as ultimately achieve Fano-like resonance, unidirectional scattering (Kerker conditions), and photon waveguide. We also consider the fundamental prospects of designing all-dielectric/metallic-dielectric photonic nanostructures, particularly those functional dielectric materials and all-dielectric three-dimensional assemblies.

1. Introduction

Dielectric nanoparticles that support strong electric and magnetic Mie-type resonances in the optical region have recently emerged as a promising platform for nanophotonic applications.[1–3] Dielectric materials such as Si and TiO_2 are earth-abundant and affordable, and they are compatible with metal-oxide-semiconductor fabrication.[4] With their high permittivity and low extinction coefficients, dielectric nanoparticles can circumvent significant ohmic losses inherent to plasmonics and serve as an energy-efficient alternative in nanophotonic design. As plasmonic nanoparticles primarily support electric resonance, realization of strong magnetic resonance in plasmonic structures is fundamentally limited to specifically designed split-ring resonators (SRRs). By comparison, dielectric nanoparticles possess multipolar electric and magnetic eigenmodes and thus offer additional routes to achieve multimodal resonant modes.[1,5] The interplay and interference between electric and magnetic modes, with the latter playing a central role, have proven useful in tailoring scattering resonance for enhanced local density of electromagnetic states and directional radiation.[6] These features have made dielectric nanoparticles promising subwavelength building blocks for a broad range of applications, such as nonlinear optics,[7–9] sensitive biosensors,[10,11] nanolasers,[12–14] and lab-on-chip photonic devices,[15–18] among others.

The electromagnetic response behavior of small dielectric particles has been rendered reliable since the original work by Gustav Mie.[19] Subsequently, a number of papers dealing with metamaterials based on dielectric particles and light-scattering properties of high-refractive-index dielectric cylinders were published.[20–23] However, it was not until 2010 that the significant magnetic response of dielectric nanoparticles in the visible range was theoretically investigated.[24] Several years after the magnetic aspects of available resonances received special attention, the concept of “magnetic light” was proposed and demonstrated in detail in both theoretical and experimental terms.[25,26] Thereafter, many studies were performed at the fundamental level, which led to the potential capacity to fabricate dielectric nanoparticles with magnetic Mie-type resonance in the visible,[27] infrared (IR),[28] and even microwave[29] spectral ranges.

Over the past decade, substantial research efforts have been devoted to dielectric nanoresonators and precise control over their optical properties.[30–32] An in-depth understanding of fundamentals behind these optical features elucidates the characteristics of resonant modes and their interactions and guides the construction of low-loss nanophotonics.[33] Specifically, resonant dielectric nanoparticles that encompass both discrete entities and compact, simplified geometrical configurations are beneficial for fundamental analysis. These nanomaterials are ideal building blocks for the construction of complex nanophotonic structures, such as optical antenna arrays and by extension, metasurfaces.[7,34,35]

This review provides an overview of experimental and theoretical advances in manipulating the scattering resonance of dielectric nanoparticles and their complex assemblies in the visible and near-IR (NIR) spectral ranges. Major breakthroughs achieved over the last decade are summarized in Figure 1.[26,36–46] Considerable attention is devoted to underlying basic concepts that serve as the fundamental framework for controlling the optical properties of subwavelength dielectric nanoparticles in comparison to their plasmonic counterparts. We also discuss the influence of a single nanoparticle's refractive index and geometry on its optical response. A significant emphasis is placed on strategies employed to achieve on-demand control over scattering characteristics, including multicolor magnetic scattering, far-field scattering efficiency, the local near-field density of states, and directional radiation patterns. We further elaborate on multimodal interference of nanoparticles with progressive complexity — starting with the coupling within discrete nanoparticles, to dielectric dimers and oligomers, one-dimensional (1D) and two-dimensional (2D) particle assemblies, dielectric-plasmonic hybrid structures. Moreover, we consider exciton coupling and discuss a plethora of peculiar optical properties, such as unidirectional forward-to-backward scattering, tunable Fano resonance, splitting resonance coupling, and photon waveguiding. Finally, we consider the prospects and challenges for all-dielectric and metal-dielectric structures, particularly those excited state-active materials and three-dimensional (3D) metastructures.

2. Fundamental Considerations

2.1. Theory Foundation

The optical response from spherical metallic and dielectric nanoparticles can be evaluated using analytical solutions derived from multipolar Mie theory, which was developed by Gustav Mie in 1908.[19] According to the classical problem described in this theory, both metallic and dielectric subwavelength spheres immersed in a medium and exposed to radiation exhibit scattering resonance at specific frequencies. The generated scattering fields can be expanded in a multipole series, characterized by electric and magnetic Mie coefficients a_n and b_n, respectively:[47]

$$E^S = \sum_{n=1}^{\infty} E_n\left(i a_n \mathrm{N}_{e\,ln}^{(3)} - b_n \mathrm{M}_{o\,ln}^{(3)}\right) \quad (1)$$

where the explicit expressions for E_n, the vector multipoles M, N and the explanation of their indices can be found in ref. 35. The Mie-scattering coefficients a_n and b_n of a dielectric sphere with a (possibly complex) refractive index n immersed in a uniform medium of refractive index n_m and size parameter x are as follows:

$$a_n = \frac{m\Psi_n(mx)\Psi'_n(x) - \Psi_n(x)\Psi'_n(mx)}{m\Psi_n(mx)\xi'_n(x) - \xi_n(x)\Psi'_n(mx)} \quad (2)$$

$$b_n = \frac{\Psi_n(mx)\Psi'_n(x) - \mathrm{m}\Psi_n(x)\Psi'_n(mx)}{\Psi_n(mx)\xi'_n(x) - m\xi_n(x)\Psi'_n(mx)} \quad (3)$$

The functions $\Psi_{n,}$ ξ_n are Riccati–Bessel functions:

$$\Psi_n(\rho) = \rho j_n(\rho), \ \ \xi_n(\rho) = \rho h_n^{(1)}(\rho) \quad (4)$$

where j_n and $h_n^{(1)}$ are the usual spherical Bessel and Hankel functions, respectively, and

$$m = n/n_m \quad (5)$$

$$x = \frac{\pi d_p n_m}{\lambda} \quad (6)$$

where d_p denotes the diameter of the nanoparticle and λ is the wavelength of the incident light.

Notably, the expansion coefficients a_1 and b_1 correspond to the basic scattering amplitudes of the electric and magnetic dipole (ED and MD) modes, respectively, whereas a_2 and b_2 correspond to quadrupolar modes. Using the abovementioned formulas, we can calculate the electric field anywhere around the sphere, but it is often convenient to express the overall response using the extinction, scattering, and absorption efficiencies as follows:[19,30]

$$Q_{ext} = \frac{2}{x^2}\sum_{n=1}^{\infty}(2n+1)Re\{a_n + b_n\} \quad (7)$$

$$Q_{sca} = \frac{2}{x^2}\sum_{n=1}^{\infty}(2n+1)(|a_n|^2 + |b_n|^2) \quad (8)$$

$$Q_{abs} = Q_{ext} - Q_{sca} \quad (9)$$

As this review aims to address the manipulation of the resonance spectral positions and modes in nanoparticles, we confine the discussion of mathematical expressions to key indicators that dictate the scattering efficiency of nanophotonic systems. We recommend that inquisitive readers refer to well-received publications by Kerker, Bohren, and Huffman, which report on vigorous studies conducted to derive analytical solutions to the classical problem of the sphere.[47,48] As the original publication was written during a period of great interest in colloidal science and because of computational limitations in the early 20th century, only the exact solution for the scattering problem was provided for spherical particles at that time.

To analyze the resonance characteristics of nonspherical particles, it is worth noting that they are related to fundamental physical parameters, such as the dimension and refractive index, and specific

features of the geometry under consideration. In such cases, the multipolar decomposition technique must be employed to elucidate interferences between various modes.

A small collection of early studies dating back to the late 1940s established a theoretical foundation for understanding and predicting the optical properties endowed by dielectric structures, ranging in scale from single nanoparticles to metasurfaces.[49–51] As the field continues to advance, extensions of the classical approach have been proposed, and each iteration either provides new insights on the parameters of importance to achieve targeted optical properties or seeks to simplify the inherently long computing processes. Some typical methods include, but are not limited to, the T-matrix method, multiple multipole method, and discrete dipole approximation.[52–59] A modern interpretation of Mie theory through the multipolar decomposition approach was demonstrated by Butakov and Schuller,[60] who proposed the concurrent use of numerical and experimental methods. They considered additional design parameters, including the aspect-ratio of dielectric structures and the substrate refractive index under experimental conditions. These studies have provided insights into how these structural parameters affect the multipole scattering behavior and enable the optical properties of complex dielectric structures to be predicted.

2.2. Magnetic Response

Optically-induced magnetic field components in natural materials are intrinsically weak.[61] In the case of metal nanoparticles, the resonant modes originate from their surface plasmon resonance, where the oscillations of free electrons in the conduction band near the metal surface give rise to a strong, dominant electric field. However, a magnetic field with comparable strength is relatively difficult to obtain but is desirable for attaining the notable effects mentioned in the Introduction. In this section, we briefly outline two strategies that enable the manifestation of a strong magnetic field. The first is the coupling of the plasmonic nanoparticle to an external MD emitter. The magnetic component of the emitter is then amplified by the near-field effects of plasmonic nanoparticles. Such an emitter can serve as a direct source of magnetic fields or constitute a gain medium. Rare-earth ions are, in this case, ideal emitters with robust MD modes owing to their *4f*-orbitals and abundant intra-*4f*-optical transitions, which allow extensive spectral coverage ranging from the ultraviolet (UV) to NIR regime.[62–65] For instance, Eu^{3+} is often used as a magnetic dipole because of its $^5D_0 \rightarrow {}^7F_1$ MD transition, which falls in the visible range (~ 610–620 nm).[66–68]

The second approach comprises internal modification of metallic nanostructures. The generation of a magnetic field requires a proximal electric field to support the magnetic dipole and store magnetic energy. Conventional circuits use components, such as inductors and capacitors, to generate and strengthen the magnetic field. An equivalent of such circuits at the microscopic level involves

introducing a dielectric gap into the nanostructure. At the resonant frequency, this gap enables the magneto-inductive coupling of the incident radiation by inducing charge separation of the resonant current, which is reminiscent of a capacitor.[69] The most outstanding design of this type is the SRR, devised by Pendry et al. in 1999 (Figure 2a).[5,70] Since then, various designs have been proposed, such as single U-shaped rings, nanocups, and a split ball resonator as a 3D equivalent of an SRR.[58,71–73] Typically, these plasmonic SRRs display resonance with a spectral dependence that varies linearly with their physical dimensions. Thus, scaling the nanoantenna's size allows resonance frequencies to be tuned over a wide range from gigahertz and terahertz to the territory of optical frequencies.[74–76] However, SRRs function better in the IR spectral range and mostly fail in the visible regime because of high fabrication cost and increased radiation loss.

As a viable alternative, dielectric nanoparticles can support a strong magnetic Mie-type resonance with low energy loss, even with simple geometrical shapes such as spheres, cylinders, and cubes (Figure 2b).[5,26] The scattering cross-section of the MD mode in high-refractive-index dielectric nanoparticles has proven comparable to that of the ED mode.[29,77] For an isolated spherical particle, the MD resonance occurs under a specific-wavelength excitation: $\lambda = 2nR$,[4] where λ is the resonance wavelength in free space; R and n are its radius and refractive index, respectively. This relationship highlights two interesting points for discussion. First, the size-dependent magnetic resonance response rationalizes the fact that dielectric nanoparticles must be sufficiently small to generate resonance at the blue-end of the visible region. This explains why the resonance in the visible region can be achieved using dielectric nanoparticles with diameters of approximately 100–200 nm. Second, it indicates the choice of dielectric materials with composition directly related to the refractive index. These parameters are of paramount importance for designing small integrated devices while ensuring strong magnetic dipole resonance in the visible range. The scaling properties of high-refractive-index materials lead to nanoantennas with dimensions of hundreds or even tens of nanometers and an unaffected scattering response.

Apart from spherical particles, a strong, tunable magnetic response can occur in dielectric structures with other geometries such as disks or nanowires.[78] In 2007, Schuller et al. presented an experimental proof of magnetic resonance in the mid-IR region from phonon-polaritonic silicon carbide (SiC) microrods; this was followed by subsequent work based on germanium (Ge) and silicon (Si) nanowires.[20,79,80] These early studies reported that the resonance observed in such dielectrics was primarily dominated by absorption, which inhibited scattering. The development of dielectric nanophotonics gained significant momentum in the early 2010s, with the emergence of strong scattering from Si nanoparticles and cylindrical nanoantennas. High-refractive-index dielectric

nanoparticles with diameters ranging 100-250 nm exhibited strong magnetic- and electric-like responses in both visible and NIR regions.[25,26] The induced MD and ED modes can be clearly distinguished from smulation results of the electricmagnetic near-field districtution within dielectric nanoparticles.[81]

2.3. The Energy Conservation Perspective

Khurgin explained why plasmonic resonance in the NIR and visible regions constitutes a puzzle.[61] There is an assumption that miniaturization of SRR could enable resonance in the visible spectrum due to the linear dependence of resonance frequency with the dimensions of SRR. However, beyond the 100-THz range, the linear scaling breaks down and saturation ensues, which is an open problem that has been considered by Zhou et al.[82] It was reported that standard SRRs are unable to reach dimensions smaller than 35 nm, for which a magnetic resonance occurs at 900 nm because of intrinsic plasma frequency. The magnetic response in the visible range must be achieved by introducing multiple cuts into the SRR basic structure.[83]

Although further cuts can be introduced to increase the current operational bandwidth or use multiple SRRs for further miniaturization, the nanofabrication process limits practical achievements, especially when the SRR size is already small.[84] Another potential problem limiting practical implementation is energy loss. For instance, Johnson et al. demonstrated that 100-nm single SRRs based on aluminum can achieve magnetic resonance at 530 nm. However, other studies indicated that aluminum is a viable material only in the blue and UV ranges because the interband transition at 800 nm makes it extremely lossy when operating in the red portion of the visible and NIR regions.[85,86] Moreover, defect-related scattering caused by imprecise nanofabrication also undermines optical performance.

To address the probelm of energy dissipation, an examination of its constitutive parameters is necessary:[87]

$$\widehat{\varepsilon_r} = \varepsilon_r + i\varepsilon_r'' = \hat{n}^2 = (n + iK)^2 \quad (10)$$

where $\widehat{\varepsilon_r}$and $\hat{n}$ denote the complex relative permittivity and complex refractive index, respectively. The imaginary part of the permittivity, ε_r'', is the damping factor or loss parameter, whereas the corresponding part of the refractive index, K, is the extinction coefficient. They are related to one another by these simple expressions: $\varepsilon_r = n^2 - K^2$ and $\varepsilon_r'' = 2nK$.[87]

By comparing the commonly used gold (Au), silver (Ag), and copper (Cu) plasmonic materials and the archetypical high-refractive-index Si material (Figure 2c-e),[88,89] it can be observed that

metallic materials are often characterized by large damping factors. Accordingly, they induce large energy loss during wave transmission. A notable exception among metals is Ag, a low-refractive-index alternative to Si, as both incur a similar magnitude of energy loss in the visible region (Figure 2e). However, previous experimental results showed that the optical performance of Ag thin films is significantly hindered by water vapor and oxygen degradation during deposition, because the energy loss in plasmonics is highly dependent on surface roughness.[88,90]

In comparison to noble metals, Si is far more energy-efficient and has a larger refractive index, a necessity to attain large field enhancement. More importantly, the optical response observed for all-dielectric nanoantennas is entirely driven by the displacement current. Thus, they do not experience the drawback of energy dissipation due to the kinetic motion of conduction electrons and self-inductance issues in the plasmonic counterparts.[61,91,92]

2.4. Multipole Modes and Multipolar Interference

As implied by Mie theory, apart from the fundamental ED and MD modes, dielectric nanoparticles with large enough refractive indices and size parameters exhibit higher-order multipolar modes that feature a series of sharp resonance peaks, including but not limited to electric quadrupole (EQ) and magnetic quadrupole (MQ) moments.[93,94] Figure 2f shows the scattering cross-section of a 100-nm-diameter nanosphere made of a high-refractive-index dielectric material (n = 4). There are four resonance peaks in the visible region, which can be assigned to the MD, ED, MQ, and EQ modes (spanning low to high energies).[6]

Compared to plasmonic SRRs, one notable difference exhibited by high-refractive-index nanoparticles is the appearance of magnetic multipolar modes, such as MQ and magnetic hexapole (MH) moments. Traditionally, SRRs and their equivalents, such as nanoring configuration, have been designed to improve spectral purity based on the magnetic dipole contribution as their multipolar terms are mostly electric in nature.[95] The observation of multipole moments in dielectric resonators and metamaterials designed from these building blocks provides us with previously conceived modes but unattainable on experimental grounds.[93,94]

Recently, high-order multipole contributions have received an increasing amount of attention because of their special resonance features. For instance, for both dielectric spheres and cylinders, higher-order multipolar modes usually display a sharper spectral profile than a primitive dipole mode. These features are common to both electric and magnetic modes due to the symmetry of Maxwell's equations.[40,96–98] In addition, it has been demonstrated that the higher-order Mie-resonant modes exhibit two trending features in the far-field scattering: first, the number of lobes is multiplied, with

some lobes showing signs of directional far-field scattering along the preferred axes; second, the lobes of the higher-order modes become narrower. These multipole lobes (both electric and magnetic type) bestow dielectric nanoantennas with tailoring scattering patterns, which can in turn enable on-demand optical functions, such as efficient radiation steering in the nanoscale range.[99,100]

Beyond exhibiting distinct electric or magnetic modes, the resonance interference among different Mie-type modes enables tunable optical characteristics and unique scattering patterns, such as unidirectional far-field scattering and Fano-like resonance. When the ED and MD moments of a dielectric nanoresonator are excited simultaneously with comparable strength, the ratio of forward-to-backward scattering can be controlled, as theoretically discussed by Kerker et al.[101,102] An extreme case concerning the role of multipoles in far-field scattering was presented by Liu et al., who reported that with increased contributions from electric and magnetic multipoles (e.g., quadrupoles and hexapoles), scattering patterns with high directionality can be achieved to the extent of complete suppression of the side- and-back scattering lobes.[103] In addition, by tuning the interference between the narrow resonant mode and broad nonresonant mode using an electric or magnetic response, a sharp Fano resonance with characteristic asymmetric scattering can be achieved in dielectric particles and their assemblies.[39,104,105]

By extension, dielectric elements with optimized multipole excitations can be periodically patterned as metasurfaces and then equipped with novel characteristics, such as near-perfect transmission and absorption as well as negative refractive indices. For interested readers, this topic is covered in great detail in recent literature reviews by Liu and Kivshar.[102,106] These reviews also introduce the less known third member of the multipole family, namely the toroidal (TD) moment. In dielectric particles, the TD mode originates from a circulating magnetic field with an electric poloidal current distribution, as supported by symmetrical structures with a high refractive index (typically $n \geq 3.0$).[107] Moreover, benefiting from the similar scattering patterns of ED and TD modes, when the two modes become simultaneously excited with an identical but antiphase scattering magnitude, their radiation scatterings may nullify each other, resulting in an invisible state known as nonradiating anapole.[108] The efficient excitation of the nonradiating anapole make dielectric particles ideal as building blocks in the development of metamaterials with extremely high-quality factors and enhanced absorption efficiencies.[108–111]

3. Manipulation of the Scattering Characteristics

3.1. Engineering the Refractive Index

According to Mie theory (briefly described in Section 2.1), the refractive index is a crucial parameter for tuning scattering characteristics. Typically, effective Mie-type resonance is exhibited in dielectric nanoparticles with a high refractive index. For dielectric particles with a larger refractive index than the surrounding medium, both field enhancement and the quality factor will improve. Such a large index contrast tends to reduce radiation leakage from nanoparticles. Thus, the choice of materials to promote such interesting properties is very important. However, traditional fabrication processes (top-down techniques) for high-refractive-index nanostructures (e.g., Si nanoresonator) are usually complex, expensive, and difficult to apply on a large scale. This has led to a resurgence in novel fabrication strategies and alternative materials with added functionalities. In this review, we categorize dielectric nanoparticles into three classes based on the refractive index of materials: high-refractive-index dielectric (HRID) nanoparticles ($n \geq 3.0$), moderate-refractive-index dielectric (MRID) nanoparticles ($1.7 \leq n \leq 3.0$), and low-refractive-index (LRID) dielectric nanoparticles ($n \leq 1.7$). Table 1 summarizes dielectric particles with different refractive indices and optical characteristics. We will demonstrate these specific examples accordingly.

3.1.1. HRID Nanoparticles

As briefly discussed in Section 2.3, Si is perhaps the most frequently studied HRID material in the visible and IR ranges owing to its relatively low cost and the low imaginary portion of the refractive index. In recent decades, many shape-controlled fabrication techniques have been exploited to tune the Mie resonance of Si nanoparticles, with the ultimate goal of enabling entirely new avenues of research in nanophotonics. Let us first discuss the methods for Si nanoparticle fabrication.

The earliest experimental observations of scattering resonance in the visible and IR spectral ranges were demonstrated in dielectric semiconductor microrods and nanorods.[112,113] In 2012, a strong magnetic response originating from the dipolar mode of spherical Si nanoparticles was independently demonstrated by Arseniy and Evlyukhin, who established the foundation of our current understanding of magnetic Mie resonance.[25,26] Following this milestone, various fabrication techniques have been gradually developed to produce high-quality, reproducible Si nanoparticles.[31,114,115] Top-down techniques have been extensively used, such as conventional photolithography and electron beam lithography (EBL) techniques that allow reproducibility and control over particle size, shape, and position.[116,117] The downside of these lithography-based techniques is their complex, time-consuming procedure, especially for large-scale nanopatterning. As another dominant fabrication technique, laser printing also allows precise control over the size and positioning of Si nanospheres.[118–120] The main advantages of this approach are relatively high productivity and lack of harmful chemical wastes. It should be noticed that implementation of laser

printing requires high-quality laser radiation with high pulse stability, perfect beam shape, and excellent focusing. Chemical methods are attractive because they enable high-throughput fabrication of Si nanoparticles. One such method is chemical vapor deposition using disilane or trisilane as the gas precursor.[28,121] The prepared hydrogenated amorphous Si (a-Si:H) particles with relatively uniform sizes and spherical shapes can be well dispersed into solutions. However, these a-Si:H particles require post-deposition vacuum annealing to preserve their high refractive index.

In the abovementioned studies, various colors generated by Si nanoparticles with different Mie-type resonances and far-field scattering spectra have been characterized using a dark-field microscope in imaging mode or spectroscopic mode. In recent work, Si nanospheres with controllable diameters (ranging 95-200 nm) were synthesized via the solid-state disproportionation of SiO into Si and SiO_2.[27] The obtained nanospheres exhibited good quality with high uniformity of shape, high crystallinity, and narrow size distribution. The vivid colors of the Si nanospheres dispersed in the solution allowed one to recognize with the naked eye a variable range that spanned the visible blue to orange. These scattering colors, which depend on the diameter of Si nanospheres, were observed at the single-particle level in dark-field images (Figure 3a). The detailed decomposition of Mie-type modes with respect to their resonant peaks was analyzed against MD and ED moments located in the NIR range.

In addition to boosting far-field scattering, dielectric nanoparticles can provide enhanced electric and magnetic near-field local state densities.[40,122–124] Such near-field amplitudes and phases of localized optical modes can be characterized via apertureless near-field scattering optical microscopy (ANSOM). In an earlier work, the deep-subwavelength hotspot of a disconnected Si nanodisk was mapped to a four-lobed mode pattern, which was assigned to the contribution of an EQ mode by comparing the simulated radiation pattern.[40] Moreover, Kivshar et al. experimentally discriminated the optically induced resonance of both magnetic and electric modes in discrete Si nanoparticles through an approach that combined both polarization-resolved dark-field spectroscopy and ANSOM measurements.[122] Moreover, by using a polarization- and angle-resolved cathodoluminescence setup based on scanning transmission electron microscopy, Habteyes et al. successfully visualized the internal field of the selected degenerate electromagnetic modes from a single-object antenna, including the radial higher-order modes (Figure 3b,c).[124] Meanwhile, a high degree of radiation directionality was also obtained for this antenna, benefiting eigenmode interference. The directionality could be controlled by changing the direction of the incident light or the type of source.

According to Kerker's scattering framework (briefly mentioned in Section 2.4), single dielectric nanoparticles with a high refractive index have the potential to generate either forward- or backward-

scattered fields as soon as their magnetic and electric modes become coherent, resulting in unidirectional light scattering.[29,36,125] The experimental verification of Kerker's conditions for a single dielectric particle, held in the microwave region, was first demonstrated in 2011.[29] Later, Fu et al. presented an experimental study on the anisotropic scattering of Si nanoparticles in the visible region. They showed that the obtained forward scattering strongly dominates its backward counterpart more than six times across a broad spectral range (Figure 3d).[36] Another related work also experimentally demonstrated the Kerker-type zero backward scattering from GaAs pillars in the red spectral segment.[125]

Apart from Si nanoparticles, semiconductors with a refractive index of > 3 in groups IV and III-V, such as Ge, GaSb, and GaP, are potential candidates for achieving Mie-type scattering once assembled in nanostructures.[114] The associated optical features hinge on their extinction coefficients and refractive indices across a specific wavelength range. For example, Mie-type dipole resonance was experimentally observed in the visible spectrum using GaAs nanodisks[125] and in the mid-IR spectral range using lead telluride (PbTe) nanoparticles.[126]

Most of the abovementioned studies focused on passive dielectric structures with functionalities hardly modifiable during fabrication. With the increasing demand for tunable optical devices, there has been a wave of innovation in optical materials displaying tunable resonance in response to external stimuli.[127] For example, some HRID materials are sensitive to the environmental temperature, thus enabling dynamic control of the refractive index. Lewi et al. took advantage of the large refractive index ($n \cong 6$) and the large temperature change coefficient of PbTe to achieve the reversible tuning of Mie resonance in such nanoparticles.[128] Another example was demonstrated in $Ge_2Sb_2Te_5$ (GST) nanostructures. The crystallization of the GST materials was modulated through a phase transition, which varied the refractive index. Tian et al. experimentally demonstrated continuous tuning of anapole states of GST disks in the mid-IR spectral range by partial crystallization of bulk materials (Figure 4a).[129]

In addition to conventional semiconductors, transition metal dichalcogenides (TMDs) have recently gained the spotlight owing to their excitonic properties and high refractive index (~ 4). This creates new opportunities to investigate interactions between Mie-type resonant modes and excited polaritons. Only last year, Shegai et al. managed to illustrate the novel concept of TMD nanoantennas using WS_2 nanodisks, which were fabricated by an exfoliation-EBL-etching process.[37] By varying the nanodisk dimensions to spectrally overlap the Mie-type anapole mode with the concomitant exciton transition in the same nanostructure, the coupling and hybridization between these two resonant features would be enabled (Figure 4b).

3.1.2. MRID Nanoparticles

In contrast to HRID nanoparticles, which are normally prepared based on complicated top-down fabrication techniques under cleanroom conditions, most MRID nanoparticles are synthesized through bottom-up chemical approaches that are attainable in synthesis labs. Although some MRID materials are not entirely loss-free, their absorption efficiency in the visible spectrum is still noticeably lower than that of metals (e.g., Au, an archetypical metallic material). They constitute a suitable class of materials for the Mie resonance study. In fact, prior to the Information Age, which brought about an increased interest in Si, most light-scattering experiments were performed on colloidal particles with moderate refractive indices.[130]

In 2015, Lin et al. assessed the effects of refractive index and size change of nanospheres on their Mie-resonance properties.[41] According to the simulated scattering patterns obtained as a function of the refractive index (Figure 5), all Mie resonance shifts to the red portion as the index increases. Moreover, with a refractive index value fixed at either 2.7 or 3.5, the resonance shifts to the red with increasing particle size. Furthermore, the spectral features of higher-order resonance modes become more obvious. As with their HRID counterparts, MRID nanoparticles also support magnetic resonance tuning, though the strength of their MQ mode and other high-order modes are often too minuscule to be considered. Resonators based on MRID materials are less energy efficient compared to Si and GaAs, but this drawback can be largely compensated by facile preparation methods, the plurality of material choices, and their versatile applications.[2]

Among the members of MRID materials, titanium dioxide (TiO_2) has been widely used in consumer goods such as paints, sunscreens, and food additives, among other applications.[131] As a semiconducting material with a refractive index between 2.5 and 2.8, TiO_2 is regarded as a low-loss, high-performance material that can serve as an alternative to Si and provide Mie resonance in the visible range.[132–136] Wang et al. successfully characterized the optical resonant properties of TiO_2 spheres using dark-field scattering measurements at the single-particle level and provided a detailed theoretical analysis based on Mie-theory simulations (Figure 6a).[137] They presented an extensive study of the changes induced by a crystalline phase variation on their optical response. This study considered variations in particle size, internal structure, and refractive index. Given the long development history of this class of materials, the fabrication strategies for TiO_2 nanostructures have matured and diversified beyond the classical wet chemistry used for colloidal synthesis. These new strategies, such as e-beam lithography and the template-assisted assembly method, enable the nanofabrication of metasurfaces.[134,138] Recently, efforts have been undertaken to develop TiO_2

metasurfaces as color filters for emitter enhancement and reflection coatings on existing architectures, especially solar cells.[131,138,139]

Cuprous oxide (Cu_2O) materials, with a refractive index typically close to 2.7, was initially developed as a photocatalyst material given its electronic properties.[41,140,141] However, in recent years, Cu_2O spheres have been further employed as nanoantennas in the visible range because large-scale production of these spheres with a uniform diameter can be easily synthesized through wet-chemistry methods.[142,143] Their role as Mie-type resonators dates back to 2015 when Lin's group experimentally and theoretically demonstrated that the electric and magnetic modes (up to quadrupolar) in Cu_2O spheres can spectrally overlap. As such, they have the potential to become highly efficient Huygens elements. They exhibit directional scattering, as evident by their examination, particularly by that of $Au@Cu_2O$ core-shell nanostructures under a dark-field microscope. The evolution of the forward-to-backward scattering ratio at the scattering peak of $Au@Cu_2O$ has also been shown to depend on the diameter of the entire nanostructure (Figure 6b).[41]

Perovskites are another interesting family of MRID materials and can be broadly categorized into oxides and halides. Whereas oxide perovskites have been extensively used in electrooptics for modulation purposes owing to their intrinsic crystal structure, which endows them with high second-order electric susceptibility (χ^2) coefficients, recent studies have revealed that such noncentrosymmetric materials can exhibit Mie resonance-activated efficient second harmonic generation (SHG).[144,145] New studies have emerged in this area in recent years and revealed that these activated processes in $BaTiO_3$ and $LiNbO_3$ nanoparticles are produced through solvothermal processes.[146–149] For instance, an increase in the size of $BaTiO_3$ nanoparticles shifted the SHG peak to the red portion (600 nm) due to the influence of the MD mode, whereas $LiNbO_3$ was demonstrated to operate in the near-UV region. More materials can be used to explore suitable candidates that feature peculiar optical properties and cover the far-red and IR region.

Halide perovskites have attracted increased interest due to their facile synthesis and potential for large-scale use in many technological applications.[45,150,151] Halide perovskites are materials with a typical ABX_3 composition, where A stands for an organic or inorganic cation, B stands for the central cations (that typically host Pb^{2+}, Sn^{2+}, or Ge^{2+}), and X stands for halide ions (Cl^-, Br^- or I^-), which are mostly responsible for color tuning in the visible range. Markedly different from oxide perovskites, halide perovskites with a refractive index between 2 and 3 support optical resonances and provide excitonic states in nanostructures at room temperature with high photoluminescence quantum yield.

In halide perovskites, light sources can be directly located within the nanoresonator wherein the largest near-field enhancement occurs. This feature expands the possibilities for discovering novel

types of light sources and nano-lasers for nanophotonic applications.[151,152] Additionally, as a multifunctional resonant structure, the mutual interplay between Mie resonances and excitons allows, on the one side, to manipulate the optical states of the internal excitons through Mie resonances and, on the other side, to adjust the exciton scattering characteristics of the perovskite. In 2018, Tiguntseva et al. reported the observation of broadly tunable Fano resonances in halide perovskite nanoparticles ($MAPbBr_3$) by coupling a narrow exciton resonance to a broader cavity resonant mode.[45] The characteristics of the scattering spectrum with Fano-line shape are observed in the dark-field spectra of isolated nanoparticles and the extinction spectra of particle lattice (Figure 6c). Notably, through the chemical tuning of the exciton resonance, a reversible tuning of the Fano resonances in the visible optical range was realized, opening novel opportunities for the realization of active nanophotonic structures.

3.1.3. LRID Nanoparticles

Owing to ineffective light confinement in LRID nanoparticles with a lower refractive index than that of the surrounding medium, isolated LRID nanoparticles, such as polymer spheres and colloidal SiO_2 particles, are usually optically inactive in the visible and near-IR regions. At present, the conventional method to functionalize this class of materials for optical scattering involves the synthesis of hollow nanostructures with extremely thin low-refractive-index shells, as best demonstrated by Retsch and his coworkers using hollow silica spheres.[153] The physics behind this design is simple: the efficiency of Mie resonance is maximized through a hollow-structure design because this design significantly lengthens the mean free path of light while multiple scattering events within the "photonic glass" are reduced. However, because of the intrinsically low refractive index of these nanostructures, their optical properties are especially sensitive to morphology; hence, precise control of the synthesis process is required.

To enhance the Mie resonance of low-refractive-index nanoparticles, Guo and his co-workers introduced a metal dressing approach that is strong enough for visual mapping and still highly sensitive to design variations.[154] The metal shell serves as a high-reflection boundary (i.e., a reflective mirror at the single-particle level) to support tight field confinement within the volume of the nanoparticle. According to the theoretical analysis, the scattering peak was assigned to the enhanced transverse electric (TE_{11}) mode of the low-refractive-index nanospheres, which created strong circulating displacement currents to generate magnetic modes of considerable strength (Figure 6d). Given the leaky behavior of LRID materials in terms of resonance, Khudiyev and coworkers demonstrated nonresonant Mie scattering by using core-shell polymer nanowires comprising

polyvinylidene difluoride and polycarbonate. In this manner, they could tackle the radiant loss and achieve directional scattering in the visible and NIR regions.[155]

When LRID nanoparticles are arranged in 2D or 3D assemblies, they enable optical response in both visible and NIR ranges, such as multicolor reflections.[156–159] Significantly different from Mie-type resonance exhibited by individual HRID nanoparticles, the optical response from LRID 2D- or 3D-ordered assemblies results from photonic band gaps induced by periodicity. Through periodic modulation of the refractive index between the constituent nanoparticles and the surrounding medium, the propagation of light is prohibited at certain wavelengths and in specific directions within the structure, thereby constituting a photonic bandgap (directional or omnidirectional). In such systems, Mie-resonance is barely discernible.

In 2015, Yuan et al. reported a novel strategy for fabricating structurally colorful colloidal fibers.[160] Periodically nanostructured colloidal fibers have shown tunable structural colors under dark-field imaging. The occurrence of such homogeneous and noniridescent structural colors has been attributed to two phenomena: Mie scattering of the colloidal spheres and the reflection of photonic crystals through the photonic bandgap effect. This finding demonstrated the possibility of observing Mie-type scattering in assemblies of low-refractive-index materials, but this work lacked a detailed and comprehensive analysis of the underlying physical mechanism.

Another work by Rybin et al. on photonic crystals and dielectric metamaterials demonstrated that a periodic photonic structure can be transformed into a metamaterial by finely tuning the composition, dimension, geometry, and symmetry of the building blocks.[161] However, this concept remains to be experimentally validated in dielectric structures using subwavelength building blocks.

3.2. Geometrical Design

The geometry of dielectric nanoparticles is an essential factor in designing a nanoresonator with desirable optical features. The early work by Mongia and Bhartia in 1994 laid the foundation of geometrical design, which included tuning the shape and size ratio and using the core-shell concept.[51] As of today, many dielectric nanoantenna and metasurface designs still use this work as a source of inspiration and technical reference. In this section, we present a few case studies wherein the observed optical phenomena have shown striking dependence on geometry.

Until now, our discussion has been mainly focused on spherical particles. Owing to their isotropic, dielectric structures, nanospheres have the potential to be employed as isotropic antennas with easily switchable directionality, irrespective of the illumination axes,[122] and remain excellent candidates for the study of novel optical phenomena such as superdirectionality and invisibility.[99,107]

However, similar to what occurred in nanoplasmonics, electromagnetic resonance in dielectric nanoparticles are worth considering beyond the framework of spherical models. Typically, whereas isotropic spheres continue to be used for fundamental research, the design of anisotropic shapes may lead to novel dielectric nanoantennas and metasurfaces. The reason for using nonspherical particles in real-world applications is twofold. First, lithography-based methods for constructing dielectric nanostructures can hardly be applied to spherical nanoparticles. Equivalents such as dielectric nanodisks and cylinders are more practical alternatives as they can be patterned onto substrates using current nanofabrication techniques.[162–165] Second, nonspherical geometries offer a high degree of geometrical freedom, potentially leading to anisotropic electromagnetic resonance.

The strength and resonant wavelength of magnetic and electric dipoles are closely related to the geometry of dielectric nanoparticles. In that regard, tuning their size ratios constitutes an excellent strategy for investigating the overlap of ED, MD, and other higher-order modes, beneficial to directional scattering. For example, Kivshar et al. developed a directional optical antenna with a high forward-to-backward scattering ratio by tuning the diameter-to-height aspect ratio of Si nanodisk to 1.35.[116] In the same vein, a generalized model has been proposed that extends to spheroid geometries as well as cylindrical and parallelepiped shapes. In fact, with an increase in the aspect ratio from 1, the ED and MD resonances approach each other and fully merge at 2.086, maintaining minimum backward scattering at the resonance of total scattering for particles with a refractive index of 3.5 (Figure 7).[166]

These two significant developments establish the fundamental design principle for the geometric fine-tuning of dielectric nanoantennas. Other exciting designs have been demonstrated based on asymmetric dielectric structures, including nanowires, and V- and L-shaped nanoantennas.[167–171]

By introducing a cavity into the antenna, the geometric design concept was further extended to include hollow-based dielectric nanoantenna architectures to realize better and more flexible control over the overlapping of magnetic and electric modes.[109,172,173] The initial experimental results suggest that, given a specific cavity-to-nanoantenna ratio, the gap structure may lead to an extremely enhanced local magnetic field in the center of the antenna.[174,175] However, the design of dielectric nanoparticles that produce high-order multipole scattering (e.g., octopole, hexadecapole) but suppressed dipole modes remains a challenging task. Typically, the contribution of high-order multipole modes to resonance in the visible region is negligible compared to intense low-order modes (e.g., ED and MD modes). A recent attempt by Zenin et al. presented an intuitive means of designing dielectric nanoparticles with enhanced high-order resonance by introducing a cavity. They showed that both ring and core-shell nanostructures supported almost pure high-order multipole scattering.[175]

The electric and magnetic fields of dielectric structures can efficiently couple to dipole emitters. Although the electromagnetic fields of plasmonic nanoparticles are primarily concentrated at the surface, the magnetic field of dielectric particles can fully penetrate their structures and reach field maxima inside the particles. In traditional dielectric nanoparticles, the regions of high magnetic local density of states are unavailable for positioning optical emitters.[176,177] Recently, researchers have sought to address this issue using well-designed structures, and a widely used strategy is to place quantum emitters into a nanocavity in the center of the nanoantenna.[176,178–180] High Purcell factors within dielectric nanoparticles are useful for enhancing magnetic light emission, promising the next-generation of miniaturized magnetic light sources. Although this seems to be an elegant solution, many proposed designs are only based on numerical methods and without experimental evidence. Achieving such proof suffers from probing techniques that only allow the positions of emitters to be fixed in the cavity with the broad uncertainty of hundreds of nanometers.[181] Alternatively, organized arrangements of coupled dielectric nanoparticles, dimers, and oligomers can be considered viable options.[182] We will now turn to the discussion of such coupling effects in dielectric nanoresonators.

3.3. Coupling Effects

Although tuning of the refractive index and geometry of dielectric nanoparticles has been employed as the trial-and-error strategy for manipulating scattering properties in line with Mie theory and its expanded models, the intrinsically weak scattering of individual nanoparticles remains a problem. Moreover, it has been challenging to realize the desired multipole-mode interference in complex hybrid resonant nanostructures or to provide suitable hotspots for coupling with optical emitters. The coupling between all-dielectric nanoresonators or dielectric nanoparticles and either substrates or excitons has been demonstrated to address these challenges, giving rise to unique functionalities such as stronger far-field scattering cross-section,[183–187] directional Fano resonance,[39,104,188–190] subwavelength waveguiding,[43,191,192] splitting resonance phenomenon,[44,193] and near-field confined local state density.[42,194–196] In this section, we review recent advances in the manipulation of scattering characteristics beyond single-level resonators through the coupling effects that result from various particle dispositions, including but not limited to dimers, oligomers (trimers, tetramers, and hexamers), hybrid arrangements, and 1D/2D assemblies. Moreover, the coupling effects between nanoparticles and supporting substrates or excitons are also briefly discussed.

3.3.1. Dielectric Dimers

Research on hybridization began with dimeric structures owing to their simplicity in terms of both design (simulations) and practical realization. The earliest research progress theoretically showed that coupling of dielectric nanoparticles in dimers produced new hybridized resonant modes. A

dipole−dipole model was employed to simulate electrodynamical interactions responsible for their optical properties.[194] When two Si nanospheres interact in close proximity (approximately tens of nanometers), their elementary ED and MD resonances hybridize to form bonding and antibonding modes similar to plasmonic dimers, resulting in homogenous electric-electric, magnetic-magnetic, as well as heterogenous electric-magnetic modes. Meanwhile, Si dimers numerically exhibit excellent magnetic field enhancement under specific light polarization, which is not observed in their plasmonic counterparts. Quantitative studies show that all-dielectric dimers can generate hotspots with field strength six times stronger and nonradiative loss 94% less than their identically designed plasmonic counterparts.[42] The spectral positions and widths of their resonant bands depend on the radii of nanoparticles and their relative separation distance.[183] In higher-order multipole modes, a modified hybridization theory must be introduced to describe their complex interactions.[197] This modified hybridization theory, based on Maxwell's equations for non-Hermitian composite systems, overcomes the limitation by considering the following three factors: magnetic interaction, retardation effect, and radiation loss. These factors dictate dielectric scattering, mode coupling with the incident radiation, radiative strength determination, and scattering resonance broadening.

On the experimental side, a series of fabrication techniques and characterization methods have been employed to investigate Si dimers, such as EBL techniques and dark-field images.[183,198] Some expected optical properties, including tunable scattering spectra,[199] polarization-dependent far-field radiation,[183] and enhanced near-field hotspots, have been successfully characterized in detail.[42,200] Notably, Bakker et al. experimentally observed the hotspots of the magnetic field in the visible region using the incident light polarized across the nanodimer primary axis.[42] Reinhardt and co-workers demonstrated switchable, uniform chiroptical hotspots in Si nanodisk dimers by combining experimental spectroscopy and electromagnetic simulations.[201]

In Section 3.2, while dealing with a geometric design, we mentioned that scattered light can be routed by dielectric structures, depending on the excitation wavelength and geometric design of the dielectric antennas. This is notably the case for a V-shaped Si nanoantenna.[169] However, directional V-shaped antennas are only responsible for controlling the scattering of light propagating to the substrate at normal incidence, rather than longitudinal excitation. The tunable control of directional scattering along the substrate could be useful for developing optical nanocircuits capable of linearly transporting both electrons and light.[202] Drawing upon knowledge gained from rigorous studies on nanoplasmonics, many of the established design principles can be incorporated into dielectric nanodesigns. One such design can be realized using a pair of asymmetric nanoparticles.[203,204] Albella et al. theoretically demonstrated tunable directional scattering using an asymmetric Si dimer upon

excitation.[203] To explore this possibility, a routing structure comprising three dimers was designed, and its near-field intensity was simulated using the finite-difference time-domain (FDTD) method. By virtue of variability in the sizes of the two nanoparticles, the MD resonance of one particle was adjusted to overlap with the ED resonance of the other; this enabled an electric-magnetic coupling with directional scattering. The same group further experimentally demonstrated this concept through a back focal plane imaging system combined using a prism-coupling technique.[202] The fabricated asymmetrical Si dimers exhibited switchable directional scattering triggered by the excitation wavelength (Figure 8a). This unique light-steering structure can be used as a nanoscale routing element for electromagnetic radiation.

In contrast to Fano resonance arising from the overlap between the ED and quadrupolar mode in plasmonic meta-atoms, a Si-nanosphere dimer was experimentally and theoretically demonstrated as an excellent alternative to support directional magnetic-based Fano scattering.[188] Owing to the overlap of the broad ED mode and the narrow MD mode in the Si dimer, deformation of these two modes enabled suppressed backward scattering and enhanced forward scattering from the structure. The resulting Fano resonance is superior to that from a single Si sphere and is likely to expand the scope of application toward signal monitoring and external modulation.

3.3.2. Dielectric Oligomers

Compared to dielectric dimers, dielectric oligomers provide increased structural diversity with precise control over optical properties — such diversity results in more complex hybridization in electric and magnetic modes. Apart from the size and spacing of constituent particles, the geometric configuration also influences mechanical coupling. Yan et al. demonstrated magnetically induced transparency in Si nanosphere oligomers,[184] wherein the coupling between the MD resonance and broad electric gap mode contributed by electric dipoles from the individual spheres led to suppressed reflection. In their work, both experimental and theoretical analyses were performed by comparing two types of trimers with different aggregation states, which belonged to D_{3h} (equilateral triangle) and $D_{\infty h}$ (linear arrangement) symmetry groups. In the D_{3h} trimer, owing to its trigonal planar geometry, the centralized charge area has the same effect on the displacement current of all three spheres. Thus, the magnetic responses from the three spheres reach their maximum value simultaneously, leading to a Fano antireflection dip. Conversely, the $D_{\infty h}$ group's linear geometry permits hotspots to be generated at only two junctions such that the alternating charge distribution weakens the magnetic resonance energy, which in turn explains the origin of the two shallow dips observed in the spectra (Figure 8b).

In practice, particle oligomers (plasmonic, dielectric, and even hybrid) are often employed as platforms for facilitating the investigation of Fano resonance owing to their flexible geometric

organization. In the early 2000s, plasmonic oligomers were found to be among the most robust structures to exhibit Fano resonance in the visible and NIR regions.[205,206] By breaking the structural symmetry of metallic oligomers, it is possible to induce resonant interference between a collective subradiant dark mode and the superradiant collective bright mode; this ultimately results in a characteristic asymmetrical line shape in the scattering spectra associated with Fano resonance. Similar to plasmonic nanostructures, Fano resonance has also been reported for the oligomers of dielectric nanoparticles.[39,104,105,207] However, differences can be observed in their electric and magnetic field distributions. First, in the plasmonic case, the field enhancement is mainly generated between particles such that the enhancement factor is susceptible to the separation distance. In the case of dielectric nanoparticles, the field is concentrated inside particles and can be harvested by placing a particle at the center of the oligomer**.** Second, in dielectric oligomers, the MD resonance of discrete dielectric particles is dominant in the emergence of Fano resonance, whereas ED resonance is responsible for their plasmonic counterparts.

Kivshar and his co-workers theoretically established the existence of Fano resonance in all-dielectric oligomers.[104] Through spectral simulation of various particle configurations from tetramers to heptamers, they found that the spectral position of Fano resonance generated by coupled dielectric nanoparticles is mainly determined by the magnetic dipole of the centrally positioned particle. Unlike their Au equivalents, Si heptamers' resonance response hardly depends on their structural variations. The experimental observation of Fano resonance in all-dielectric oligomers was achieved by the same group, utilizing heptamers made of millimeter-scale ceramic spheres.[105] A coupled ED-MD approximation showed that such Fano resonance occurs due to interference between the resonance (narrow) mode of the central sphere and the nonresonant (broad) mode created by the collective response of the six-sphere ring. They also established a relationship between the near- and far-field properties of Fano resonance. In the same year, this Fano-resonance concept was further extended to Si oligomers by controlling the size of the centrally positioned nanodisk.[39] The obtained Fano resonance was produced with the incident light propagating in a direction normal to the oligomer plane. In this configuration, the generation of Fano dips is primarily due to MD coupling of individual nanoparticles.

Interestingly, the same group also reported distinctive magnetic−magnetic Fano resonance from a dielectric tetramer under the incident light with the electric field polarization and propagation direction both lying in the plane of oligomer.[207] Different from previous reports, such Fano resonance originates from interference between individual MDs of discrete nanoparticles and an optically

induced collective MD mode. In particular, this MD mode is generated by the collective circulation of electric displacement currents around disjoined particles (Figure 8c).

In the experimental arena, with the development of lithographic technologies and the increasing variation of methods, a low-cost, scalable, facile colloidal lithography technique was developed to fabricate HRID oligomers composed of randomly positioned nanodisks.[208] Distinct from ordered oligomers, the random nanostructure presents an ultra-broadband (300−1,200 nm) directional light scattering, which can be used for photovoltaic and optoelectronic applications.

3.3.3. Hybrid Particle Arrangements

Peculiar optical features can emerge by combining the specificities of metallic and dielectric structures, as mentioned in Sections 2.2 and 2.3. For instance, efficient interference between electric and magnetic dipoles requires the intensity of these two modes to be identical. Typically, the ED resonance of metal nanoparticles is much stronger than that of dielectric counterparts, whereas the MD resonance in dielectric nanoparticles is intrinsically stronger than that in metal counterparts. Therefore, interference of the ED and MD modes from these two counterparts can lead to large anisotropic scattering ratios and strong electromagnetic fields.[186,209]

The unidirectional light scattering of metal-dielectric heterodimers comprising Si and Au spheres has been theoretically and experimentally reported.[186,189,210] The frequency regime of unidirectional scattering is determined by the coupling between ED and MD modes with a small spectral shift, which can be achieved by adjusting the size and spacing of the two spheres (Figure 8d).[46] As the incident light is parallel to the radial direction of the heterodimers, the scattering strength can also be enhanced. As an alternative, MRID dielectric spheres (such as boron nanospheres) have been coupled to Si nanoparticles. In a boron-based heterodimer, the intrinsic and broad resonant band of boron nanospheres is easily coupled to adjacent narrow modes, enabling precise and independent tailoring of the radiation pattern via tuning of the particle size.[211] Specifically, changing the size of the boron nanosphere can adjust the broad mode of the hybrid structure, resulting in the fine control of its scattering properties, whereas tuning the size of the Si spheres can adjust the narrow mode and lead to the coarse tuning of their scattering (Figure 8d). Furthermore, Sun et al. theoretically predicted that if the sizes of dielectric and metal constituents as well as their gap distance can be delicately tuned to match both amplitudes and phases of the electric and magnetic dipole moments, a nearly ideal first Kerker condition at the resonance wavelength can be expected, yielding highly efficient unidirectional forward scattering with a forward-to-backward scattering ratio of ~ 48 dB.[212]

In addition to heterodimers, composite structures comprising metal and dielectric nanoparticles have also been reported in other architectures, such as hybrid Au-dielectric particle clusters,[213] SiO_2@Si arrays coated with Au-nanoparticles,[195] plasmonic nanosponges filled with Si,[185] and Au@ZnS core-shell nanostructures.[189] Among these designs, Kucherik et al. demonstrated a hybrid structure of Si spheres covered with Au nanoclusters, which were pre-fabricated in liquid phase under laser irradiation.[213] Coating of Au nanoparticles enhances the local near-field density and resonant light absorption of these complex nanoresonators. Another typical composite is the core-shell structure with Au particles as the core and with dielectric ZnO materials as the shell.[189] This inverted hybrid architecture makes it possible to achieve prominent Fano resonance through the coupling between the ZnS shell's broad scattering background and the narrow plasmon resonance of the Au core.

3.3.4. 1D and 2D Assemblies of Dielectric Nanoparticles

The miniaturization of photonic devices and efficient transportation of electromagnetic energy are two primary considerations for designing integrated photonic circuits. Traditional dielectric waveguides can achieve almost lossless light propagation but usually suffer from the diffraction limit. The waveguide's lateral dimension must be greater than half of the wavelength of the guided wave, which makes miniaturization of waveguide structures difficult.[214] Therefore, guiding photon energy in 1D or 2D arrays at nanoscale is of considerable significance in physics and optics.

The practical realization of 1D arrays of dielectric nanoparticles for subwavelength guiding has been considered in numerous studies.[43,191,192] Nanoscale waveguiding occurs when resonance from one particle to another is coupled through dipole−dipole interaction along the particle chain.[43] Such systems are distinct from subwavelength grating waveguides and 1D photonic crystals in the sense that discrete components must be resonant at the wavelength of interest rather than requiring a collective periodic interaction.

Although dielectric particle-based waveguiding is stringent in particle size, many studies have reported that the propagation distance in these systems is much larger than in plasmon arrays.[214–216] In particular, Quidant et al. numerically designed and experimentally demonstrated a subwavelength waveguide with a propagation distance of several micrometers using assembled TiO_2 nanowire chains.[215] In addition to linear propagation, optical signals circulate antenna corners and split with Y-type structures. It has been numerically demonstrated that light propagates in bent periodic dielectric waveguides at angles up to 180° in a highly efficiency manner.[214,216,217]

Savelev et al. theoretically investigated electromagnetic energy transport in 1D dielectric particle chains modeled as continuous MD and ED arrays.[191] Moreover, they numerically analyzed both the

linear and nonlinear propagation of pulses (solitary waves) in chains of HRID dielectric nanoparticles.[192] They demonstrated waveguiding through resonant Si nanoparticle chains within the visible region by applying advanced fabrication and characterization techniques. As particles are arranged in a 1D periodic structure, the magnetic resonance coupling between adjacent particles leads to photon energy transport along the particle chain, with the propagation distance exceeding 500 μm (Figure 8e).[43] Such a proof of concept validates the possibility of developing nanolasers using a linear chain of simple nanostructures as nanoantennas.[218]

2D dielectric nanostructures, commonly known as metasurfaces, are best described as artificial electromagnetic media consisting of periodic subwavelength building blocks, used collectively to manipulate light on a large scale. Compared to detached dielectric resonators, they offer a platform for engineering electric and magnetic response through multimodal interference and collective coupling based on thin-layer structures, bestowing metadevices with many intriguing optical properties,[8,10,17] such as amplitude and phase control of scattering modes.[17,219,220] However, a detailed discussion of these metasurfaces does not fall within the scope of this review. Interested readers are therefore encouraged to refer to relevant review papers (among others) in order to apprehend the concepts and developments of such metasurfaces and metamaterials.[3,5,218] To date, the fabrication of dielectric metasurfaces with exquisite subwavelength elements remains a pertinent problem due to widely used top-down methods such as lithography being complex, expensive and limited in large-scale production. Here, we wish to highlight an early work performed by Shi et al., in which 2D arrays of Si spheres were fabricated using a bottom-up self-assembly approach, which supports a sizeable magnetic response in the NIR region with small optical loss (Figure 8f).[121] Further advances on this work could lead to breakthroughs in bottom-up processing of large-area, easily fabricated metamaterials that work in the NIR region.

3.3.5. Substrate Coupling Effects

While the majority of theoretical studies consider isolated spherical particles or their clusters in free space, nanoparticles are normally affixed or strongly coupled to a substrate for practical application.[162] The interaction with the substrate will substantially modify their magnetic and electric responses, providing an on-demand additional degree of freedom in tailoring their optical properties, which is useful in many photonic applications, such as surface-enhanced spectroscopy and optical antenna design.

Both analytical and numerical studies of the influence of substrate on electromagnetic resonance remain challenging, largely because different simulation methods may yield divergent outcomes. Mie theory has been widely used for the analysis of dielectric nanoparticles in a homogenous medium or

free space, but not applicable for the particles adhered to substrates. Alternatively, a comprehensive numerical study of substrate effects on the spectral response of HRID nanoparticles was conducted using the FDTD method.[221] Specifically, three simulation models, namely particles in free space, particles on a dielectric substrate, and particles on a perfect electric conductor (PEC), have been taken into account in the analysis of substrate effect. By comparing the simulated scattering spectra, the authors claimed that the dielectric substrate slightly attenuated the dipole resonance but strongly suppressed the higher-order resonance, as compared to the free-space model. In contrast, the PEC substrate shifted the spectral resonance wavelength of the nanoparticles and changes their scattering cross-section to a large extent. In another study, Miroshnichenko et al. proposed a new analytical approach through the use of Green's dyadic function and a point-dipole approximation.[222,223] By doing so, researchers were able to observe new substrate-related magnetoelectric features, such as magnetoelectric coupling, resonance-frequency renormalization, and resonant bianisotropy.

Coupling effects have inspired researchers to actively control the optical properties of dielectric nanoresonators by varying substrate materials.[190,224] Specifically, the combination of Si spheres with a high refractive index and VO_2 thin films with a reversible phase transition has provided possibility for active resonance tuning (Figure 9a).[190] The scattering cross-sections contributed by ED and MD modes vary to different degrees when the VO_2 substrate undergoes an insulator-to-metal phase transition (Figure 9b), as a result of a change in the refractive index. The tunable feature makes this structure promising for functioning as a nano-level light source with adjustable illumination intensity or as a nanoantenna with assorted signals.[162]

Although plasmonic nanostructures on dielectric substrates have become commonplace, such as Ag or Au nanoparticles inserted in Si solar cells for conversion enhancement, coupling of dielectric nanostructures onto metal substrates remains rarely investigated.[225–228] Compared to dielectric substrates, metal substrates have negative permittivity, which leads to different coupling effects. Theoretical speculation, based on a mirror-image-induced mode, has been applied to understand interactions between dielectric particles and plasmonic substrates.[229] When dielectric nanoparticles are positioned on a flat metallic mirror, the dipole-dipole interaction between EDs of dielectric resonators with their mirror image counterparts results in effective magnetic polarization currents and a huge enhancement of the scattering cross section at specific frequencies. The origin of this induced magnetic dipole is similar to that appearing in metallic cut wire pairs. The arrangement of dielectric nanoparticles and a metallic substrate in close proximity enables incoming electromagnetic plane waves to be converted into evanescent waves, which excite surface plasmons at the metal surface and confine them into the gap region. This localization of fields creates a "hotspot" of concentrated

electromagnetic energy in the gap.[230,231] Experimental proofs of significant near-field enhancement and large field confinement have been demonstrated using dielectric nanosystems. The generated hotspots have been further employed to perform surface-enhanced Raman spectroscopy.[196,232] The gap size between dielectric nanoparticles and substrates affects the degree of near-field interactions, allowing possibility for optimization of field confinement.[38,196,233] For instance, in a particle-on-film system, a spacer layer of Al_2O_3 thin film was obtained using atomic layer deposition, with the distance between the Si nanodisk and Au substrate controlled by varying the spacer thickness (Figure 9a).[38] A decrease in spacing enhanced the capability of the Au substrate in tailoring the resonance coupling, and the corresponding scattering peak red-shifted (Figure 9c).

In a parallel study, Sinev et al. indicated that both enhanced scattering cross-sections and amplified local fields inherent to the particle-on-film configuration can be controlled by using polarized incident light. Employing dark-field spectroscopy, they observed polarization-controlled transformation from a narrow resonance (MD scattering with high-quality factor) to a broadband resonance (ED mode),[187] accompanied by a switch in the near-field local state.

3.3.6. Coupling with Excitons

The absorption and emission behaviors of optical emitters, such as dye molecules and 2D materials, can be modified by tailoring their surrounding local electromagnetic environments.[181,233,234] Both metallic and dielectric nanostructures are good candidates for providing such local environments.[235,236] In most cases, investigations are focused on the effects of electromagnetic media on luminescent centers. However, when optical emitters are positioned closely to resonant nanoantennas, their excitons may coherently interact with resonance modes to form new hybrids. This phenomenon, known as resonance coupling, has stimulated extensive research, owing to its importance in fundamental research and nanophotonic applications, such as quantum information processing, exciton-polariton lasing, and all-optical switching.[237–240]

Over the past decade, resonance coupling has been widely investigated in heterostructured systems comprising metallic nanoparticles and dye molecules with spectrally overlapped plasmonic and excitonic resonance.[241] Dielectric nanoresonators feature negligible quenching effects and the ability to support both electric and magnetic resonance modes in the visible range, making them particularly suitable for resonance coupling. This resonance coupling originates from the coherent energy exchange between emitters and nanoresonators.

The action of coherent energy transfer in dielectric-emitter systems was first observed experimentally in Si nanospheres coated with J-aggregate molecules.[44] The hybridization of

resonance modes dampened the scattering spectrum, indicative of a characteristic resonant coupling. In particular, appropriate molecular parameters were selected to illustrate the resonance approaching a strong coupling regime, which resulted in anticrossing with a mode splitting of 100 meV. Furthermore, a mode splitting of 300 meV, determined from the minimum distance between the anticrossing branches of hybridized modes (Figure 9d), was also observed for Cu_2O nanospheres coated with rhodamine-640 aggregates (Figure 9a).[193]

Investigations of resonance coupling in heterostructures composed of 2D exciton-coupled Si nanospheres in a monolayer semiconductor have also been performed. It has been theoretically demonstrated that resonance coupling is possible through energy transfer between dielectric resonators and exciton emitters, allowing anticrossing with a mode splitting of 43 meV.[224] This result validates the weak coupling regime, whereas a robust coupling regime is achievable in a similar structure by changing the surrounding dielectric medium from air to water.[242] In experimental terms, a particle-on-film design involving deposition of silicon nanospheres onto a monolayer of WS_2 was employed (Figure 9a), which exhibited a Fano interference with unidirectional light scattering and temperature-controlled tunability (Figure 9e).[224]

Resonance coupling has also been investigated in structures with nonspherical shapes, such as the coupling between dye aggregates and Si disks.[243] The mutual independence of ED and MD resonance in Si nanodisks could be harnessed to distinguish excitonic coupling in different resonance modes. The anticrossing with ED and MD modes shows different mode-splitting intensities of 60 ± 3 and 68 ± 2 meV, respectively. Other dielectric nanoresonators with complex topological structures, such as Si nanogrooves, have also been used in combination with molecular excitation for generating unidirectional Fano resonance.[244]

Different from those systems with emitters externally coupled to dielectric resonators, resonators comprising multifunctional dielectric materials embedded with luminescent emitters, such as perovskite[45] and TMD materials, have also been described.[37] The resulting exciton resonant band can be tuned to overlap Mie-type resonance, leading to tunable Fano resonance or hybrid modes with strong coupling.

4. Emerging Applications

Over the past few years, the rapid development of dielectric nanostructures with multimodal functionalities has allowed a wide range of nanophotonics applications, such as surface enhanced sensing,[245,246] nanospectroscopy,[247] nanolasers,[13,151] nonlinear optics,[9,248] and photovoltaic devices.[15] In this section, we attempt to highlight the broad utility of dielectric nanoparticles for

diverse optical effects based on the individual particles or isolated particle arrangements, including enhancing optical nonlinearity and manipulating the luminescence of both antenna materials and surrounding emitting materials.

4.1 Enhancing Optical Nonlinearity

Strong Mie-type resonances manifested in all-dielectric resonators have proven effective as suitable candidates in enhancing nonlinear effects at the nanoscale due to the intense electromagnetic fields confined within the nanoparticle entity or multi-particle arrangements. In contrast to plasmonic structures, the geometrical resonances of dielectric nanoparticles can support the mode volume for nonlinear effects not limited to interfaces, beneficial for higher conversion efficiencies.[249]

The study of third harmonic generation (THG) dates from the early 1970s based on works by Burns and Bloembergen. At that time, silicon was considered to be promising material for THG due to its strong optical absorption.[250] However, the conclusions from this pioneering work were based on bulk films. In recent years, as the preparation of silicon nanoparticles become possible with advances in nanotechnology, Kivshar and his co-workers were able to study the nonlinearity of Si nanodisks through resonant mode engineering.[251] In the vicinity of the magnetic dipolar resonance, the locally enhanced electromagnetic fields result in two orders of magnitude enhancement of third harmonic signal with respect to bulk silicon. In the following year, coupling effects between Si nanodisks arranged in the dielectric trimers provided an additional degree of freedom in tuning nonlinear response with a strong reshaping of the third-harmonic spectra.[251] Furthermore, a multifold enhancement of the THG was realized by the resonant excitation of high-quality collective modes in quadrumers composed of Si nanodisks.[252] Another coupling effect on the THG was demonstrated in a hybrid structure composed of a resonant subwavelength Si nanowire and Si nanodisk.[253] By placing the nanodisk at optimized separation from the nanowire, the third harmonic intensity was modulated by a factor of up to 4.5. Apart from Si particles, Maier and his co-workers theoretically and experimentally examined the efficient third harmonic response of isolated Ge nanodisks excited at their anapole modes.[254,255]

Normally, the efficiency of the coupled light emission that corresponds to a certain resonant mode will largely depend on both the overall designed optical structures and the spatial properties of the pumping source. As a result, both the strength and multipolar composition of the excited harmonic fields can be manipulated by tailoring the spatial vectorial structure of the excitation beam onto the nanoresonator structure. The nonlinear fields with different radiation states can be addressed in subwavelength Si nanoparticles by exciting different types of multipolar Mie resonances, leading to either an enhanced or suppressed nonlinear magnetic response.[255] Recently, Fedyanin et al.

demonstrated the role of the collective magnetic multipole modes in nonlinear optics through an oligomeric formation of Si quadrumers. As a single entity, the quadrumer is fundamentally limited by its high degree of geometrical symmetry and hence the excitation of linearly polarised beams is optically inefficient. Cylindrical beams, with characteristics of azimuthal and radial components, can break such dark modes which resulted in an enhancement of the THG signal by up to two orders of magnitude.[256]

Silicon is a centrosymmetric material and hence the studies of nonlinear optical properties of Si nanoparticles have been mainly targeted on THG effects. However, in 2017, Makarov et al. successfully fabricated the nanocrystalline Si nanoparticles with a highly efficient second-order nonlinear response by employing an optimized laser printing technique.[257] There are several different polycrystalline grains separated by a net of interfaces in these laser-printed nanoparticles, which give rise to the enhanced second-order optical response owing to local breaking of inversion symmetry. Meanwhile, as mentioned in previous section 3.1.2, some oxide perovskites with relatively high second-order electric susceptibility (χ^2) coefficients, like $BaTiO_3$ and $LiNbO_3$ nanoparticles, were explored for efficient SHG effects in both visible and UV region.[146,147] Recently, Savo et al. developed three-dimensional disordered microspheres by the bottom-up assembly of $BaTiO_3$ nanocrystals and demonstrated their broadband and simultaneous Mie-enhanced SHG over a wavelength range of 100 nm.[149]

Similar to the directional Mie scattering, the modulation of the radiation pattern and polarization states of the nonlinear response is essential to realize the full potential of designed dielectric nanoantennas. Morales et al. demonstrated efficient SHG in AlGaAs nanoantennas which showed the possibility to generate a bidirectional second harmonic radiation pattern and produce complex vector polarization beams.[258] Furthermore, the importance of the crystalline orientation in dielectric nanoantennas for unidirectional SHG emission was revealed by Xu et al., as they attained all-optical nonlinear switching between forward and backward emission by the active modulation of SHG in (110)-grown GaAs nanoantennas.[259] Traditionally, the nonlinear response of dielectric nanoparticles is observed largely by employing lower-order geometrical resonances that often result in low Q factors ($Q < 100$). Recently, a new physical mechanism, called bound states in the continuum (BIC), for suppressing radiative losses of individual nanoscale resonators was implemented to engineer special modes with high-quality factors.[9] The BIC mode can significantly boost nonlinear effects for increasing SHG efficiency in individual subwavelength dielectric resonators, which is promising for specific applications such as low-threshold nanolasers and compact quantum light sources (Figure 10a,b).

4.2 Modulating the Fluorescence of Antenna Materials

The development of dielectric nanostructures provides a new approach to effectively manipulate the fluorescent radiation characteristics of antenna materials. For instance, similar to the plasmonic structures, the enhanced electric or magnetic fields of the semiconducting dielectric resonators can enable significantly enhanced light absorption and help to generate a high-temperature electron gas. The hot electrons can radiate broadband luminescence through the intraband transition. Such hot-electron intraband luminescence was achieved in monocrystalline GaAs nanospheres when the dipolar magnetic mode of such GaAs spheres is resonantly excited by a femtosecond laser.[260]

As the most used semiconductor, silicon is known to possess excellent electronic property, but also suffers from low fluorescence quantum efficiency due to its indirect bandgap characteristics, preventing its applications in light-emitting photonic devices. In 2018, Zhang et al. showed through the engineering of nanoscale Si resonators to support the electric and magnetic resonances, it is possible to realize the white-light emission from Si nanoparticles and enhance its quantum efficiency.[261] The relaxation time of hot carriers in Si nanoparticles was dramatically increased by the magnetic and electric dipole resonances, while the radiative recombination lifetime of hot carriers was reduced by the multipolar resonant modes. As a result, the quantum efficiency of Si nanoparticles was improved by a factor of 10,000 as compared with bulk silicon. In another example, a nanoscale white-light source composed of the metal-dielectric hybrid nanoparticle was fabricated by introducing Au islands into Si nanoparticles.[247] The gold component in the hybrid architecture enhances the photoexcitation efficiency of the Si-based emitter. The enhancement was attributed to the increased optical absorption due to the surface plasmon resonance of gold and the photoinjection of hot electrons into the active material.

Combining high quantum yield of luminescence and moderate refractive index, halide perovskites are attractive for all-dielectric resonant nanophotonics and meta-optics. However, the current reported perovskites-based lasers are still restricted in the microscale. Further device miniaturization would become complicated due to inevitable radiation losses. By employing the low-order Mie-resonant mode, Tiguntseva et al. successfully demonstrated a compact room-temperature nonplasmonic nanolaser.[151] The dielectric $CsPbBr_3$ perovskites nanocubes with a feature size of 310 nm can exhibit both efficient Mie-resonant lasing and structural coloring in the visible and near IR frequency ranges and allow Mie resonances-governed single-mode lasing to be performed (Figure 10c).

The high quality factor provided by the Mie resonant dielectric nanostructures is important for realizing the miniaturized laser with a further reduction of sizes. By making use of the supercavity

modes with high quality factor, Mylnikov et al. demonstrated optically pumped lasing action in GaAs nanocylinder, which is one of the smallest all semiconductor nanolasers thus far.[13] The fundamental mechanism underlying such lasing action originates from the destructive interference between Fabry-Perot and Mie modes which can lead to a significant enhancement in the quality factor of the cavity (Figure 10d).

4.3 Manipulate the Luminescence of Surrounding Emitters

Thanks to the enhanced and confined optical local electric field, subwavelength resonators can improve the brightness and directivity of emission as well as the spontaneous decay rate of a quantum emitter located near the nanoantenna. Due to the relatively low Q-factors of individual subwavelength resonators, dimers of all-dielectric nanoparticles separated by a nanoscale gap have been used to reduce optical losses of fundamental modes and to enhance locally the intensity of the electric field. Regmi et.al reported a design of all-dielectric Si nanogap antennas capable of enhancing the fluorescence detection of single molecules.[245] The Si nanodisk dimer is optimized to confine the near-field intensity in the 20 nm nanogap, leading to a 270-fold increase in fluorescence emission signals. In another case, the efficient coupling between gallium phosphide nanodisk dimer and atomically thin two-dimensional WSe_2 results in a fluorescence enhancement exceeding 10^4 and a Raman scattering signal enhancement exceeding 10^3 (Figure 11).[262] On the other hand, not only can dimer-like Si nanoantennas enable enhancements of both fluorescence and Raman scattering signals, but also allow negligible non-radiative loss and ultra-low heat generation.[246]

The integration of plasmonic and Mie resonators in hybrid dielectric-metal antennas with nanoscale gaps embedded with quantum emitters provides an alternative and effective approach to make the ultracompact photonic light sources with enhanced performance. This novel design can overcome the problem of large optical losses in metal nanostructures and enable photon density of states larger than that in all-dielectric counterparts. In 2018, Sugimoto et.al reported on a hybrid nanoantennas consisting of a crystalline spherical Si nanoparticle on Au mirror with a monolayer of Si quantum dots sandwiched within the gap.[233] This novel design enables a photoluminescence enhancement reaching 700-fold at the hot spot. Later, Yang et al. experimentally demonstrated a 69-fold increase in the emission intensity and a 42-fold decay rate enhancement of Si quantum dots compared with uncoupled quantum dots by using similar nanoantenna.[263] Besides, the Mie resonance mode also provides flexible control of far-field radiation characteristics.

Since the high-index dielectric nanoantennas can support the electric and magnetic multipolar modes resonances at the same time, they can not only be used to control the light emission of electric quantum emitters described above, but also can be employed to manipulate the luminescence

processes of magnetic quantum emitters. In 2019, Vaskin et al. experimentally demonstrated that both electric (at 610 nm) and magnetic (at 590 nm) dipole transitions of Eu^{3+} ions can be enhanced by dielectric metasurfaces composed of Mie resonant Si nanocylinders.[264] The use of all-dielectric nanoresonators also allows selective manipulation of magnetic dipole transitions of quantum emitters. Mivelle et al. showed a selective enhancement of magnetic emission from Eu^{3+}-doped nanoparticles using a photonic nanoresonator properly designed to exhibit a magnetic resonance.[265] Very recently, Cheng et al. reported another pathway to achieve selective manipulation of the magnetic dipole transitions of Eu^{3+} ions by doping europium ions into all-dielectric sub-micrometer zirconia spheres supporting strong magnetic Mie resonances.[266] Unlike previous demonstrations that magnetic dipole emitters are placed outside dielectric nanoresonators, Eu^{3+}-doped zirconia structure enables light emitters to access the magnetic hot spot within the dielectric nanoresonator.

5. Summary and Perspective

In summary, we have outlined recent advances in manipulating resonant scattering in dielectric nanoparticles and their assemblies. The resonant properties of dielectric nanoparticles make it possible to precisely control the electrical and magnetic components of light, providing new functionalities not attainable by purely plasmonic counterparts. The future development of metaoptics based on these subwavelength dielectric building blocks is highly desirable for optoelectronic and integrated photonic applications. We attempted to pose a set of research challenges, potential trends, and future directions in this field.

First, selecting appropriate composite materials is ultimately essential to achieve highly efficient Mie resonance in the visible-to-NIR spectral range. A suitable method for integrating Mie-resonant dielectric systems with emitters is also desirable. It will allow for more rapid development of Mie-resonant systems with active/functional materials, such as the perovskite nanocrystals and TMD nanomaterials as discussed above.[37,45] Such semiconductor materials can confine emitters inside Mie resonators with maximal quality factors, which offers new opportunities for developing nanoscale light sources in integrated devices and displays.

Second, in translating dielectric nanomaterials from a scientific concept to real-world applications, 2D metasurfaces and 3D metamaterials are meaningful owing to their strong optical response and integrated structures.[267,268] However, fabrication of exquisite 2D/3D metastructure with subwavelength elements is a challenging problem. Top-down methods based on lithography are complicated and expensive, limiting the 3D spatial extension of current 2D metasurfaces or layered metamaterials developed in small settings.[269,270] The bottom-up self-assembly method holds promise for achieving large-scale, ordered 2D/3D dielectric structures, which are now hardly attainable. These

approaches may bring us a step closer to 3D Mie-resonant dielectric nanostructures with tailored optical properties, while offering opportunities to research coupling effects and multiple interference interactions within 3D periodic structures.

Meanwhile, it should be emphasized that although the emergence of all-dielectric nano-optics is an encouraging development, this does not imply the total replacement and irrelevance of nanoplasmonics. Instead, it represents a parallel path to advancing optics and photonics science for future research. An instance in which all-dielectric nanoresonators fall short is when they fail to overcome the free-space diffraction limit, which remains one of the most pertinent challenges in optics.[1] Plasmonic nanoparticles could achieve such a feat by exploiting their surface plasmon polariton modes, which can be localized or propagated with effective wavelengths smaller than $\lambda/2n$. The mechanism of coupling the propagating electric field with free carriers' kinetic motion is an enabler for feature research in nanometric light waveguiding and focusing.[271–274] Attaining the same optical features in dielectric optics has proven much more difficult. Thus far, there have been valiant efforts to address this limitation, but a convergent solution for reaching less than half of the diffraction wavelength in the nanoscale range remains elusive.[275–277] This challenge stems from the positive permittivity of dielectric materials in the desired wavelength range and the requirement for arrays or metasurfaces to induce a significant negative factor.[278,279] Hence, because there are no direct and facile methods available to induce negative permittivity at a single-particle level, hybrid nanostructures, most notably the core-shell and its equivalent designs, will become an attractive approach.

Acknowledgments

This work is supported by the Singapore Ministry of Education (MOE2017-T2-2-110), Agency for Science, Technology and Research (A*STAR) (Grant NO. A1883c0011), National Research Foundation, Prime Minister’s Office, Singapore under its Competitive Research Program (Award No. NRF-CRP15-2015-03) and under the NRF Investigatorship programme (Award No. NRF-NRFI05-2019-0003), and National Natural Science Foundation of China (21771135, 21878042, 21476040, 21276040).

Received: ((will be filled in by the editorial staff))
Revised: ((will be filled in by the editorial staff))
Published online: ((will be filled in by the editorial staff))

References

[1] M. Decker, I. Staude, *J. Opt. (United Kingdom)* **2016**, *18*, 103001.

[2] Y. Kivshar, A. Miroshnichenko, *Opt. Photonics News* **2017**, *28*, 24.

[3] S. Kruk, Y. Kivshar, *ACS Photonics* **2017**, *4*, 2638.

[4] A. I. Kuznetsov, A. E. Miroshnichenko, M. L. Brongersma, Y. S. Kivshar, B. Luk'yanchuk, *Science (80-.).* **2016**, *354*, 6314.

[5] P. Genevet, F. Capasso, F. Aieta, M. Khorasaninejad, R. Devlin, *Optica* **2017**, *4*, 139.

[6] T. Liu, R. Xu, P. Yu, Z. Wang, J. Takahara, *Nanophotonics* **2020**, *9*, 1115.

[7] B. Sain, C. Meier, T. Zentgraf, *Adv. Photonics* **2019**, *1*, 024002.

[8] Y. Yang, W. Wang, A. Boulesbaa, I. I. Kravchenko, D. P. Briggs, A. Puretzky, D. Geohegan, J. Valentine, *Nano Lett.* **2015**, *15*, 7388.

[9] K. Koshelev, S. Kruk, E. Melik-Gaykazyan, J. H. Choi, A. Bogdanov, H. G. Park, Y. Kivshar, *Science (80-.).* **2020**, *367*, 288.

[10] F. Yesilkoy, E. R. Arvelo, Y. Jahani, M. Liu, A. Tittl, V. Cevher, Y. Kivshar, H. Altug, *Nat. Photonics* **2019**, *13*, 390.

[11] A. Krasnok, M. Caldarola, N. Bonod, A. Alú, *Adv. Opt. Mater.* **2018**, *6*, 1701094.

[12] S. T. Ha, Y. H. Fu, N. K. Emani, Z. Pan, R. M. Bakker, R. Paniagua-Domínguez, A. I. Kuznetsov, *Nat. Nanotechnol.* **2018**, *13*, 1042.

[13] V. Mylnikov, S. T. Ha, Z. Pan, V. Valuckas, R. Paniagua-Domínguez, H. V. Demir, A. I. Kuznetsov, *ACS Nano* **2020**, *14*, 7338.

[14] J. C. Johnson, H. Yan, R. D. Schaller, L. H. Haber, R. J. Saykally, P. Yang, *J. Phys. Chem. B* **2001**, *105*, 11387.

[15] M. L. Brongersma, Y. Cui, S. Fan, *Nat. Mater.* **2014**, *13*, 451.

[16] M. Caldarola, P. Albella, E. Cortés, M. Rahmani, T. Roschuk, G. Grinblat, R. F. Oulton, A. V. Bragas, S. A. Maier, *Nat. Commun.* **2015**, *6*, 7915.

[17] A. Arbabi, Y. Horie, M. Bagheri, A. Faraon, *Nat. Nanotechnol.* **2015**, *10*, 937.

[18] A. Tittl, A. Leitis, M. Liu, F. Yesilkoy, D. Y. Choi, D. N. Neshev, Y. S. Kivshar, H. Altug, *Science (80-.).* **2018**, *360*, 1105.

[19] G. Mie, *Beiträge Zur Optik Trüber Medien, Speziell Kolloidaler Metallösungen*, WILEY- VCH Verlag GmbH & Co. KGaA, Weinheim, **1908**.

[20] J. A. Schuller, R. Zia, T. Taubner, M. L. Brongersma, *Phys. Rev. Lett.* **2007**, *99*, 107401.

[21] B. I. Popa, S. A. Cummer, *Phys. Rev. Lett.* **2008**, *100*, 207401.

[22] L. Cao, J. S. Park, P. Fan, B. Clemens, M. L. Brongersma, *Nano Lett.* **2010**, *10*, 1229.

[23] L. Cao, P. Fan, E. S. Barnard, A. M. Brown, M. L. Brongersma, *Nano Lett.* **2010**, *10*, 2649.

[24] A. B. Evlyukhin, C. Reinhardt, A. Seidel, B. S. Luk'Yanchuk, B. N. Chichkov, *Phys. Rev. B* **2010**, *82*, 045404.

[25] A. B. Evlyukhin, S. M. Novikov, U. Zywietz, R. L. Eriksen, C. Reinhardt, S. I. Bozhevolnyi, B. N. Chichkov, *Nano Lett.* **2012**, *12*, 3749.

[26] A. I. Kuznetsov, A. E. Miroshnichenko, Y. H. Fu, J. Zhang, B. Lukyanchukl, *Sci. Rep.* **2012**, *2*, 492.

[27] H. Sugimoto, T. Okazaki, M. Fujii, *Adv. Opt. Mater.* **2020**, *8*, 2000033.

[28] L. Shi, T. U. Tuzer, R. Fenollosa, F. Meseguer, *Adv. Mater.* **2012**, *24*, 5934.

[29] J. M. Geffrin, B. García-Cámara, R. Gómez-Medina, P. Albella, L. S. Froufe-Pérez, C. Eyraud, A. Litman, R. Vaillon, F. González, M. Nieto-Vesperinas, J. J. Sáenz, F. Moreno, *Nat. Commun.* **2012**, *3*, 1171.

[30] D. Tzarouchis, A. Sihvola, *Appl. Sci.* **2018**, *8*, 184.

[31] Z. J. Yang, R. Jiang, X. Zhuo, Y. M. Xie, J. Wang, H. Q. Lin, *Phys. Rep.* **2017**, *701*, 1.

[32] J. Yan, X. Liu, C. Ma, Y. Huang, G. Yang, *Mater. Sci. Eng. R Reports* **2020**, *141*, 100563.

[33] D. C. Tzarouchis, P. Ylä-Oijala, A. Sihvola, *IEEE Trans. Antennas Propag.* **2017**, *65*, 3184.

[34] A. Krasnok, R. Savelev, D. Baranov, P. Belov, *World Sci. Handb. Metamaterials Plasmon.* **2017**, 337.

[35] M. Panmai, J. Xiang, Z. Sun, Y. Peng, H. Liu, H. Liu, Q. Dai, S. Tie, S. Lan, *Opt. Express* **2018**, *26*, 12344.

[36] Y. H. Fu, A. I. Kuznetsov, A. E. Miroshnichenko, Y. F. Yu, B. Luk'yanchuk, *Nat. Commun.* **2013**, *4*, 1527.

[37] R. Verre, D. G. Baranov, B. Munkhbat, J. Cuadra, M. Käll, T. Shegai, *Nat. Nanotechnol.* **2019**, *14*, 679.

[38] A. Maimaiti, P. P. Patra, S. Jones, T. J. Antosiewicz, R. Verre, *Adv. Opt. Mater.* **2020**, *8*, 1901820.

[39] K. E. Chong, B. Hopkins, I. Staude, A. E. Miroshnichenko, J. Dominguez, M. Decker, D. N. Neshev, I. Brener, Y. S. Kivshar, *Small* **2014**, *10*, 1985.

[40] T. G. Habteyes, I. Staude, K. E. Chong, J. Dominguez, M. Decker, A. Miroshnichenko, Y. Kivshar, I. Brener, *ACS Photonics* **2014**, *1*, 794.

[41] S. Zhang, R. Jiang, Y. M. Xie, Q. Ruan, B. Yang, J. Wang, H. Q. Lin, *Adv. Mater.* **2015**, *27*, 7432.

[42] R. M. Bakker, D. Permyakov, Y. F. Yu, D. Markovich, R. Paniagua-Domínguez, L. Gonzaga, A. Samusev, Y. Kivshar, B. Lukyanchuk, A. I. Kuznetsov, *Nano Lett.* **2015**, *15*, 2137.

[43] R. M. Bakker, Y. F. Yu, R. Paniagua-Domínguez, B. Luk'Yanchuk, A. I. Kuznetsov, *Nano Lett.*

2017, *17*, 3458.

[44] H. Wang, Y. Ke, N. Xu, R. Zhan, Z. Zheng, J. Wen, J. Yan, P. Liu, J. Chen, J. She, Y. Zhang, F. Liu, H. Chen, S. Deng, *Nano Lett.* **2016**, *16*, 6886.

[45] E. Y. Tiguntseva, D. G. Baranov, A. P. Pushkarev, B. Munkhbat, F. Komissarenko, M. Franckevičius, A. A. Zakhidov, T. Shegai, Y. S. Kivshar, S. V. Makarov, *Nano Lett.* **2018**, *18*, 5522.

[46] H. Sugimoto, T. Hinamoto, M. Fujii, *Adv. Opt. Mater.* **2019**, *7*, 1900591.

[47] C. F. Bohren, D. R. Huffmann, *Absorption and Scattering of Light by Small Particles*, Wiley-VCH Verlag GmbH, Weinheim, Germany, **1998**.

[48] W. D. Bancroft, C. Gurchot, *J. Phys. Chem.* **1932**, *36*, 2575.

[49] L. Lewin, *J. Inst. Electr. Eng.* **1947**, *94*, 65.

[50] C. L. Holloway, E. F. Kuester, J. Baker-Jarvis, P. Kabos, *IEEE Trans. Antennas Propag.* **2003**, *51*, 2596.

[51] R. K. Mongia, P. Bhartia, *Int. J. Microw. Millimeter- Wave Comput. Eng.* **1994**, *4*, 230.

[52] E. Moreno, D. Erni, C. Hafner, R. Vahldieck, *J. Opt. Soc. Am. A* **2002**, *19*, 101.

[53] F. J. G. De Abajo, *Phys. Rev. B* **1999**, *60*, 6086.

[54] G. Gantzounis, *J. Phys. Chem. C* **2009**, *113*, 21560.

[55] M. I. Mishchenko, L. D. Travis, D. W. Mackowski, *J. Quant. Spectrosc. Radiat. Transf.* **1996**, *55*, 535.

[56] B. N. Khlebtsov, N. G. Khlebtsov, *J. Phys. Chem. C* **2007**, *111*, 11516.

[57] C. H. Hafner, G. Klaus, *COMPEL - Int. J. Comput. Math. Electr. Electron. Eng.* **1985**, *4*, 137.

[58] I. M. Hancu, A. G. Curto, M. Castro-López, M. Kuttge, N. F. Van Hulst, *Nano Lett.* **2014**, *14*, 166.

[59] M. A. Yurkin, A. G. Hoekstra, *J. Quant. Spectrosc. Radiat. Transf.* **2007**, *106*, 558.

[60] N. A. Butakov, J. A. Schuller, *Sci. Rep.* **2016**, *6*, 38487.

[61] J. B. Khurgin, *Nat. Nanotechnol.* **2015**, *10*, 2.

[62] R. D. Peacock, *Mol. Phys.* **1973**, *25*, 817.

[63] W. T. Carnall, P. R. Fields, B. G. Wybourne, *J. Chem. Phys.* **1965**, *42*, 3797.

[64] G. S. Ofelt, *J. Chem. Phys.* **1962**, *37*, 511.

[65] C. M. Dodson, R. Zia, *Phys. Rev. B* **2012**, *86*, 125102.

[66] R. Hussain, S. S. Kruk, C. E. Bonner, M. A. Noginov, I. Staude, Y. S. Kivshar, N. Noginova, D. N. Neshev, *Opt. Lett.* **2015**, *40*, 1659.

[67] S. Karaveli, R. Zia, *Opt. Lett.* **2010**, *35*, 3318.

[68] S. Karaveli, R. Zia, *Phys. Rev. Lett.* **2011**, *106*, 193004.

[69] T. D. Corrigan, P. W. Kolb, A. B. Sushkov, H. D. Drew, D. C. Schmadel, R. J. Phaneuf, *Opt. Express* **2008**, *16*, 19850.

[70] J. B. Pendry, A. J. Holden, D. J. Robbins, W. J. Stewart, *IEEE Trans. Microw. Theory Tech.* **1999**, *47*, 2075.

[71] J. B. Lassiter, M. W. Knight, N. A. Mirin, N. J. Halas, *Nano Lett.* **2009**, *9*, 4326.

[72] N. A. Mirin, N. J. Halas, *Nano Lett.* **2009**, *9*, 1255.

[73] A. I. Kuznetsov, A. E. Miroshnichenko, Y. Hsing Fu, V. Viswanathan, M. Rahmani, V. Valuckas, Z. Ying Pan, Y. Kivshar, D. S. Pickard, B. Luk'yanchuk, *Nat. Commun.* **2014**, *5*, 3104.

[74] U. B. and D. R. Tay, *Science (80-.).* **2004**, *303*, 1494.

[75] D. Bílková, *Phys. Rev. Lett.* **2000**, *84*, 4184.

[76] S. Linden, C. Enkrich, G. Dolling, M. W. Klein, J. Zhou, T. Koschny, C. M. Soukoulis, S. Burger, F. Schmidt, M. Wegener, *IEEE J. Sel. Top. Quantum Electron.* **2006**, *12*, 1097.

[77] A. García-Etxarri, R. Gómez-Medina, L. S. Froufe-Pérez, C. López, L. Chantada, F. Scheffold, J. Aizpurua, M. Nieto-Vesperinas, J. J. Sáenz, *Opt. Express* **2011**, *19*, 4815.

[78] J. A. Schuller, M. L. Brongersma, *Opt. Express* **2009**, *17*, 24084.

[79] L. Cao, P. Fan, A. P. Vasudev, J. S. White, Z. Yu, W. Cai, J. A. Schuller, S. Fan, M. L. Brongersma, *Nano Lett.* **2010**, *10*, 439.

[80] L. Cao, J. S. White, J. S. Park, J. A. Schuller, B. M. Clemens, M. L. Brongersma, *Nat. Mater.* **2009**, *8*, 643.

[81] M. Decker, I. Staude, M. Falkner, J. Dominguez, D. N. Neshev, I. Brener, T. Pertsch, Y. S. Kivshar, *Adv. Opt. Mater.* **2015**, *3*, 813.

[82] J. Zhou, T. Koschny, M. Kafesaki, E. N. Economou, J. B. Pendry, C. M. Soukoulis, *Phys. Rev. Lett.* **2005**, *95*, 223902.

[83] M. W. Klein, C. Enkrich, M. Wegener, C. M. Soukoulis, S. Linden, *Opt. Lett.* **2006**, *31*, 1259.

[84] F. Bilotti, A. Toscano, L. Vegni, *IEEE Trans. Antennas Propag.* **2007**, *55*, 2258.

[85] Y. H. Chen, A. F. Kaplan, L. J. Guo, *2010 Int. Conf. Opt. MEMS Nanophotonics* **2010**, *18*, 185.

[86] C. Langhammer, M. Schwind, B. Kasemo, I. Zorić, *Nano Lett.* **2008**, *8*, 1461.

[87] T. Nagai, Y. Kanemitsu, M. Ando, T. Kushida, S. Nakamura, Y. Yamada, T. Taguchi, *Phys. Status Solidi Basic Res.* **2002**, *229*, 611.

[88] K. M. McPeak, S. V. Jayanti, S. J. P. Kress, S. Meyer, S. Iotti, A. Rossinelli, D. J. Norris, *ACS Photonics* **2015**, *2*, 326.

[89] M. A. Green, M. J. Keevers, *Prog. Photovoltaics Res. Appl.* **1995**, *3*, 189.

[90] V. P. Drachev, U. K. Chettiar, A. V. Kildishev, H.-K. Yuan, W. Cai, V. M. Shalaev, *Opt.*

Express **2008**, *16*, 1186.

[91] J. B. Khurgin, A. Boltasseva, *MRS Bull.* **2012**, *37*, 768.

[92] E. Calandrini, A. Cerea, F. De Angelis, R. P. Zaccaria, A. Toma, *Nanophotonics* **2018**, *8*, 45.

[93] P. Grahn, A. Shevchenko, M. Kaivola, *New J. Phys.* **2012**, *14*, 093033.

[94] E. E. Radescu, G. Vaman, *Phys. Rev. E* **2002**, *65*, 046609.

[95] F. Monticone, A. Alù, *J. Mater. Chem. C* **2014**, *2*, 9059.

[96] K. Baek, Y. Kim, S. Mohd-Noor, J. K. Hyun, *ACS Appl. Mater. Interfaces* **2020**, *12*, 5300.

[97] D. A. Smirnova, A. B. Khanikaev, L. A. Smirnov, Y. S. Kivshar, *ACS Photonics* **2016**, *3*, 1468.

[98] R. Alaee, R. Filter, D. Lehr, F. Lederer, C. Rockstuhl, *Opt. Lett.* **2015**, *40*, 2645.

[99] A. E. Krasnok, C. R. Simovski, P. A. Belov, Y. S. Kivshar, *Nanoscale* **2014**, *6*, 7354.

[100] E. Rusak, I. Staude, M. Decker, J. Sautter, A. E. Miroshnichenko, D. A. Powell, D. N. Neshev, Y. S. Kivshar, *Appl. Phys. Lett.* **2014**, *105*, 221109.

[101] M. Kerker, D. S. Wang, C. L. Giles, *J. Opt. Soc. Am.* **1983**, *73*, 765.

[102] W. Liu, Y. S. Kivshar, *Opt. Express* **2018**, *26*, 13085.

[103] Wei Liu, Jianfa Zhang, Bing Lei, Haotong Ma, Wenke Xie, H. Hu, *Opt. Express* **2014**, *22*, 16178.

[104] A. E. Miroshnichenko, Y. S. Kivshar, *Nano Lett.* **2012**, *12*, 6459.

[105] D. S. Filonov, A. P. Slobozhanyuk, A. E. Krasnok, P. A. Belov, E. A. Nenasheva, B. Hopkins, A. E. Miroshnichenko, Y. S. Kivshar, *Appl. Phys. Lett.* **2014**, *104*, 021104.

[106] W. Liu, Y. S. Kivshar, *Philos. Trans. R. Soc. A* **2017**, *375*, 20160317.

[107] A. E. Miroshnichenko, A. B. Evlyukhin, Y. F. Yu, R. M. Bakker, A. Chipouline, A. I. Kuznetsov, B. Luk'yanchuk, B. N. Chichkov, Y. S. Kivshar, *Nat. Commun.* **2015**, *6*, 8069.

[108] K. Koshelev, G. Favraud, A. Bogdanov, Y. Kivshar, A. Fratalocchi, *Nanophotonics* **2019**, *8*, 725.

[109] Y. Yang, V. A. Zenin, S. I. Bozhevolnyi, *ACS Photonics* **2018**, *5*, 1960.

[110] A. A. Basharin, V. Chuguevsky, N. Volsky, M. Kafesaki, E. N. Economou, *Phys. Rev. B* **2017**, *95*, 035104.

[111] T. Zhang, Y. Che, K. Chen, J. Xu, Y. Xu, T. Wen, G. Lu, X. Liu, B. Wang, X. Xu, Y.-S. Duh, Y.-L. Tang, J. Han, Y. Cao, B.-O. Guan, S.-W. Chu, X. Li, *Nat. Commun.* **2020**, *11*, 3027.

[112] K. Seo, M. Wober, P. Steinvurzel, E. Schonbrun, Y. Dan, T. Ellenbogen, K. B. Crozier, *Nano Lett.* **2011**, *11*, 1851.

[113] G. Brönstrup, N. Jahr, C. Leiterer, A. Csäki, W. Fritzsche, S. Christiansen, *ACS Nano* **2010**, *4*, 7113.

[114] D. G. Baranov, D. A. Zuev, S. I. Lepeshov, O. V. Kotov, A. E. Krasnok, A. B. Evlyukhin, B. N.

Chichkov, *Optica* **2017**, *4*, 814.

[115] M. Abbarchi, M. Naffouti, B. Vial, A. Benkouider, L. Lermusiaux, L. Favre, A. Ronda, S. Bidault, I. Berbezier, N. Bonod, *ACS Nano* **2014**, *8*, 11181.

[116] I. Staude, A. E. Miroshnichenko, M. Decker, N. T. Fofang, S. Liu, E. Gonzales, J. Dominguez, T. S. Luk, D. N. Neshev, I. Brener, Y. Kivshar, *ACS Nano* **2013**, *7*, 7824.

[117] A. B. Evlyukhin, R. L. Eriksen, W. Cheng, J. Beermann, C. Reinhardt, A. Petrov, S. Prorok, M. Eich, B. N. Chichkov, S. I. Bozhevolnyi, *Sci. Rep.* **2014**, *4*, 4126.

[118] U. Zywietz, A. B. Evlyukhin, C. Reinhardt, B. N. Chichkov, *Nat. Commun.* **2014**, *5*, 3402.

[119] C. Zaza, I. L. Violi, J. Gargiulo, G. Chiarelli, L. Schumacher, J. Jakobi, J. Olmos-Trigo, E. Cortes, M. König, S. Barcikowski, S. Schlücker, J. J. Sáenz, S. A. Maier, F. D. Stefani, *ACS Photonics* **2019**, *6*, 815.

[120] P. A. Dmitriev, S. V. Makarov, V. A. Milichko, I. S. Mukhin, A. M. Mozharov, A. A. Sitnikova, A. K. Samusev, A. E. Krasnok, P. A. Belov, *J. Phys. Conf. Ser.* **2016**, *690*, 012020.

[121] L. Shi, J. T. Harris, R. Fenollosa, I. Rodriguez, X. Lu, B. A. Korgel, F. Meseguer, *Nat. Commun.* **2013**, *4*, 1904.

[122] D. Permyakov, I. Sinev, D. Markovich, P. Ginzburg, A. Samusev, P. Belov, V. Valuckas, A. I. Kuznetsov, B. S. Luk'yanchuk, A. E. Miroshnichenko, D. N. Neshev, Y. S. Kivshar, *Appl. Phys. Lett.* **2015**, *106*, 171110.

[123] P. Kapitanova, V. Ternovski, A. Miroshnichenko, N. Pavlov, P. Belov, Y. Kivshar, M. Tribelsky, *Sci. Rep.* **2017**, *7*, 731.

[124] T. Matsukata, N. Matthaiakakis, T. A. Yano, M. Hada, T. Tanaka, N. Yamamoto, T. Sannomiya, *ACS Photonics* **2019**, *6*, 2320.

[125] S. Person, M. Jain, Z. Lapin, J. J. Sáenz, G. Wicks, L. Novotny, *Nano Lett.* **2013**, *13*, 1806.

[126] S. Makarov, S. Kudryashov, I. Mukhin, A. Mozharov, V. Milichko, A. Krasnok, P. Belov, *Nano Lett.* **2015**, *15*, 6187.

[127] R. Paniagua-Dominguez, S. T. Ha, A. I. Kuznetsov, *Proc. IEEE* **2020**, *108*, 749.

[128] T. Lewi, H. A. Evans, N. A. Butakov, J. A. Schuller, *Nano Lett.* **2017**, *17*, 3940.

[129] J. Tian, H. Luo, Y. Yang, F. Ding, Y. Qu, D. Zhao, M. Qiu, S. I. Bozhevolnyi, *Nat. Commun.* **2019**, *10*, 396.

[130] S. M. Scholz, R. Vacassy, J. Dutta, H. Hofmann, M. Akinc, *J. Appl. Phys.* **1998**, *83*, 7860.

[131] H. J. Lin, K. De Oliveira Lima, P. Gredin, M. Mortier, L. Billot, Z. Chen, L. Aigouy, *Appl. Phys. Lett.* **2017**, *111*, 251109.

[132] C. Zhang, J. Jing, Y. Wu, Y. Fan, W. Yang, S. Wang, Q. Song, S. Xiao, *ACS Nano* **2020**, *14*, 1418.

[133] S. Sun, Z. Zhou, Z. Duan, S. Xiao, Q. Song, *Am. Chem. Soc.* **2017**, *11*, 4445.

[134] Y. Wu, W. Yang, Y. Fan, Q. Song, S. Xiao, *Sci. Adv.* **2019**, *5*, 0939.

[135] J. Y. Lee, M. C. Tsai, P. C. Chen, T. T. Chen, K. L. Chan, C. Y. Lee, R. K. Lee, *J. Phys. Chem. C* **2015**, *119*, 25754.

[136] H. Němec, C. Kadlec, F. Kadlec, P. Kuel, R. Yahiaoui, U. C. Chung, C. Elissalde, M. Maglione, P. Mounaix, *Appl. Phys. Lett.* **2012**, *100*, 061117.

[137] X. Zhuo, X. Cheng, Y. Guo, H. Jia, Y. Yu, J. Wang, *Adv. Opt. Mater.* **2019**, *7*, 1900396.

[138] D. Visser, D. Y. Chen, Y. Désières, A. P. Ravishankar, S. Anand, *Sci. Rep.* **2020**, *10*, 12527.

[139] I. Koirala, S.-S. Lee, D.-Y. Choi, *Opt. Express* **2018**, *26*, 18320.

[140] M. D. Susman, A. Vaskevich, I. Rubinstein, *ACS Appl. Mater. Interfaces* **2017**, *9*, 8177.

[141] K. Ullah, M. Habib, L. Huang, B. Garcia-Camara, *Nanomaterials* **2019**, *9*, 536.

[142] K. Ullah, X. Liu, N. P. Yadav, M. Habib, L. Song, B. García-Cámara, *Nanotechnology* **2017**, *28*, 134002.

[143] J. Bi, Y. Wu, L. Li, S. Zhang, S. Wu, *Nanoscale* **2020**, *12*, 3220.

[144] K. Frizyuk, I. Volkovskaya, D. Smirnova, A. Poddubny, M. Petrov, *Phys. Rev. B* **2019**, *99*, 075425.

[145] D. Smirnova, A. I. Smirnov, Y. S. Kivshar, *Phys. Rev. A* **2018**, *97*, 013807.

[146] F. Timpu, J. Sendra, C. Renaut, L. Lang, M. Timofeeva, M. T. Buscaglia, V. Buscaglia, R. Grange, *ACS Photonics* **2019**, *6*, 545.

[147] F. Timpu, A. Sergeyev, N. R. Hendricks, R. Grange, *ACS Photonics* **2017**, *4*, 76.

[148] C. Ma, J. Yan, Y. Wei, P. Liu, G. Yang, *J. Mater. Chem. C* **2017**, *5*, 4810.

[149] R. Savo, A. Morandi, J. S. Müller, F. Kaufmann, F. Timpu, M. Reig Escalé, M. Zanini, L. Isa, R. Grange, *Nat. Photonics* **2020**, *14*, 740.

[150] A. S. Berestennikov, P. M. Voroshilov, S. V. Makarov, Y. S. Kivshar, *Appl. Phys. Rev.* **2019**, *6*, 031307.

[151] E. Tiguntseva, K. Koshelev, A. Furasova, P. Tonkaev, V. Mikhailovskii, E. V. Ushakova, D. G. Baranov, T. Shegai, A. A. Zakhidov, Y. Kivshar, S. V. Makarov, *ACS Nano* **2020**, *14*, 8149.

[152] C. Huang, C. Zhang, S. Xiao, Y. Wang, Y. Fan, Y. Liu, N. Zhang, G. Qu, H. Ji, J. Han, L. Ge, Y. Kivshar, Q. Song, *Science (80-.).* **2020**, *367*, 1018.

[153] M. Retsch, M. Schmelzeisen, H. J. Butt, E. L. Thomas, *Nano Lett.* **2011**, *11*, 1389.

[154] J. Zhou, A. Panday, Y. Xu, X. Chen, L. Chen, C. Ji, L. J. Guo, *Phys. Rev. Lett.* **2018**, *120*, 253902.

[155] T. Khudiyev, E. Huseyinoglu, M. Bayindir, *Sci. Rep.* **2014**, *4*, 4607.

[156] Y. Zhang, B. Dong, A. Chen, X. Liu, L. Shi, J. Zi, *Adv. Mater.* **2015**, *27*, 4719.

[157] J. Zhou, J. Yang, Z. Gu, G. Zhang, Y. Wei, X. Yao, Y. Song, L. Jiang, *ACS Appl. Mater. Interfaces* **2015**, *7*, 22644.

[158] J. G. Park, S. H. Kim, S. Magkiriadou, T. M. Choi, Y. S. Kim, V. N. Manoharan, *Angew. Chemie - Int. Ed.* **2014**, *53*, 2899.

[159] D. Ge, L. Yang, G. Wu, S. Yang, *J. Mater. Chem. C* **2014**, *2*, 4395.

[160] W. Yuan, N. Zhou, L. Shi, K. Q. Zhang, *ACS Appl. Mater. Interfaces* **2015**, *7*, 14064.

[161] M. V. Rybin, D. S. Filonov, K. B. Samusev, P. A. Belov, Y. S. Kivshar, M. F. Limonov, *Nat. Commun.* **2015**, *6*, 10102.

[162] J. van de Groep, A. Polman, *Opt. Express* **2013**, *21*, 26285.

[163] M. R. Shcherbakov, D. N. Neshev, B. Hopkins, A. S. Shorokhov, I. Staude, E. V. Melik-Gaykazyan, M. Decker, A. A. Ezhov, A. E. Miroshnichenko, I. Brener, A. A. Fedyanin, Y. S. Kivshar, *Nano Lett.* **2014**, *14*, 6488.

[164] P. Spinelli, M. A. Verschuuren, A. Polman, *Nat. Commun.* **2012**, *3*, 692.

[165] A. Vaskin, J. Bohn, K. E. Chong, T. Bucher, M. Zilk, D. Y. Choi, D. N. Neshev, Y. S. Kivshar, T. Pertsch, I. Staude, *ACS Photonics* **2018**, *5*, 1359.

[166] B. S. Luk'Yanchuk, N. V. Voshchinnikov, R. Paniagua-Domínguez, A. I. Kuznetsov, *ACS Photonics* **2015**, *2*, 993.

[167] H. S. Ee, J. H. Kang, M. L. Brongersma, M. K. Seo, *Nano Lett.* **2015**, *15*, 1759.

[168] P. R. Wiecha, A. Cuche, A. Arbouet, C. Girard, G. Colas Des Francs, A. Lecestre, G. Larrieu, F. Fournel, V. Larrey, T. Baron, V. Paillard, *ACS Photonics* **2017**, *4*, 2036.

[169] J. Li, N. Verellen, D. Vercruysse, T. Bearda, L. Lagae, P. Van Dorpe, *Nano Lett.* **2016**, *16*, 4396.

[170] T. Zeng, L. Guo, L. Xu, T. Han, *J. Opt. Soc. Am. B* **2020**, *37*, 868.

[171] C. Wu, N. Arju, G. Kelp, J. A. Fan, J. Dominguez, E. Gonzales, E. Tutuc, I. Brener, G. Shvets, *Nat. Commun.* **2014**, *5*, 3892.

[172] J. Li, N. Verellen, P. Van Dorpe, *ACS Photonics* **2017**, *4*, 1893.

[173] J. Lv, H. Mu, Q. Liu, X. Zhang, X. Li, C. Liu, S. Jiang, T. Sun, P. K. Chu, *Appl. Opt.* **2018**, *57*, 4771.

[174] M. A. van de Haar, J. van de Groep, B. J. M. Brenny, A. Polman, *Opt. Express* **2016**, *24*, 2047.

[175] V. A. Zenin, C. E. Garcia-Ortiz, A. B. Evlyukhin, Y. Yang, R. Malureanu, S. M. Novikov, V. Coello, B. N. Chichkov, S. I. Bozhevolnyi, A. V. Lavrinenko, N. A. Mortensen, *ACS Photonics* **2020**, *7*, 1067.

[176] Y. Yang, B. Zhu, H. Dai, X. Sun, *Opt. Express* **2019**, *27*, 25931.

[177] T. Feng, Y. Xu, Z. Liang, W. Zhang, *Opt. Lett.* **2016**, *41*, 5011.

[178] T. Feng, W. Zhang, Z. Liang, Y. Xu, A. E. Miroshnichenko, *ACS Photonics* **2018**, *5*, 678.

[179] Y. Yang, B. Zhu, H. Dai, *J. Opt. Soc. Am. B* **2020**, *37*, 702.

[180] N. O. Länk, M. Käll, T. J. Antosiewicz, *ACS Photonics* **2019**, *6*, 1706.

[181] A. F. Koenderink, *ACS Photonics* **2017**, *4*, 710.

[182] N. Bonod, S. Bidault, G. W. Burr, M. Mivelle, *Adv. Opt. Mater.* **2019**, *7*, 1900121.

[183] U. Zywietz, M. K. Schmidt, A. B. Evlyukhin, C. Reinhardt, J. Aizpurua, B. N. Chichkov, *ACS Photonics* **2015**, *2*, 913.

[184] J. H. Yan, P. Liu, Z. Y. Lin, H. Wang, H. J. Chen, C. X. Wang, G. W. Yang, *Nat. Commun.* **2015**, *6*, 7042.

[185] A. O. Larin, A. Nominé, E. I. Ageev, J. Ghanbaja, L. N. Kolotova, S. V. Starikov, S. Bruyère, T. Belmonte, S. V. Makarov, D. A. Zuev, *Nanoscale* **2020**, *12*, 1013.

[186] H. Wang, P. Liu, Y. Ke, Y. Su, L. Zhang, N. Xu, S. Deng, H. Chen, *ACS Nano* **2015**, *9*, 436.

[187] I. Sinev, I. Iorsh, A. Bogdanov, D. Permyakov, F. Komissarenko, I. Mukhin, A. Samusev, V. Valuckas, A. I. Kuznetsov, B. S. Luk'yanchuk, A. E. Miroshnichenko, Y. S. Kivshar, *Laser Photonics Rev.* **2016**, *10*, 799.

[188] J. Yan, P. Liu, Z. Lin, H. Wang, H. Chen, C. Wang, G. Yang, *ACS Nano* **2015**, *9*, 2968.

[189] H. Chen, L. Shao, Y. C. Man, C. Zhao, J. Wang, B. Yang, *Small* **2012**, *8*, 1503.

[190] Y. Huang, J. Yan, C. Ma, G. Yang, *Nanoscale Horizons* **2019**, *4*, 148.

[191] R. S. Savelev, A. P. Slobozhanyuk, A. E. Miroshnichenko, Y. S. Kivshar, P. A. Belov, *Phys. Rev. B* **2014**, *89*, 035435.

[192] R. S. Savelev, A. V. Yulin, A. E. Krasnok, Y. S. Kivshar, *ACS Photonics* **2016**, *3*, 1869.

[193] Q. Ruan, N. Li, H. Yin, X. Cui, J. Wang, H. Q. Lin, *ACS Photonics* **2018**, *5*, 3838.

[194] P. Albella, M. A. Poyli, M. K. Schmidt, S. A. Maier, F. Moreno, J. J. Sáenz, J. Aizpurua, *J. Phys. Chem. C* **2013**, *117*, 13573.

[195] H. Yang, B. Q. Li, X. Jiang, J. Shao, *Nanoscale* **2019**, *11*, 13484.

[196] Z. Huang, J. Wang, Z. Liu, G. Xu, Y. Fan, H. Zhong, B. Cao, C. Wang, K. Xu, *J. Phys. Chem. C* **2015**, *119*, 28127.

[197] M. Pascale, G. Miano, R. Tricarico, C. Forestiere, *Sci. Rep.* **2019**, *9*, 14524.

[198] Z. Dong, T. Wang, X. Chi, J. Ho, C. Tserkezis, S. L. K. Yap, A. Rusydi, F. Tjiptoharsono, D. Thian, N. A. Mortensen, J. K. W. Yang, *Nano Lett.* **2019**, *19*, 8040.

[199] J. van de Groep, T. Coenen, S. A. Mann, A. Polman, *Optica* **2016**, *3*, 93.

[200] P. Albella, R. A. De La Osa, F. Moreno, S. A. Maier, *ACS Photonics* **2014**, *1*, 524.

[201] X. Zhao, B. M. Reinhard, *ACS Photonics* **2019**, *6*, 1981.

[202] T. Shibanuma, T. Matsui, T. Roschuk, J. Wojcik, P. Mascher, P. Albella, S. A. Maier, *ACS*

Photonics **2017**, *4*, 489.

[203] P. Albella, T. Shibanuma, S. A. Maier, *Sci. Rep.* **2015**, *5*, 18322.

[204] T. Shibanuma, P. Albella, S. A. Maier, *Nanoscale* **2016**, *8*, 14184.

[205] W. S. Chang, J. B. Lassiter, P. Swanglap, H. Sobhani, S. Khatua, P. Nordlander, N. J. Halas, S. Link, *Nano Lett.* **2012**, *12*, 4977.

[206] J. A. Fan, C. Wu, K. Bao, J. Bao, R. Bardhan, N. J. Halas, V. N. Manoharan, P. Nordlander, G. Shvets, F. Capasso, *Science (80-.).* **2010**, *328*, 1135.

[207] B. Hopkins, D. S. Filonov, A. E. Miroshnichenko, F. Monticone, A. Alù, Y. S. Kivshar, *ACS Photonics* **2015**, *2*, 724.

[208] Y. Zhang, Y. Xu, S. Chen, H. Lu, K. Chen, Y. Cao, A. E. Miroshnichenko, M. Gu, X. Li, *ACS Appl. Mater. Interfaces* **2018**, *10*, 16776.

[209] R. Jiang, B. Li, C. Fang, J. Wang, *Adv. Mater.* **2014**, *26*, 5274.

[210] A. Devilez, B. Stout, N. Bonod, *ACS Nano* **2010**, *4*, 3390.

[211] P. Liu, J. Yan, C. Ma, Z. Lin, G. Yang, *ACS Appl. Mater. Interfaces* **2016**, *8*, 22468.

[212] S. Sun, D. Wang, Z. Feng, W. Tan, *Nanoscale* **2020**, 22289.

[213] A. Kucherik, S. Kutrovskaya, A. Osipov, M. Gerke, I. Chestnov, S. Arakelian, A. S. Shalin, A. B. Evlyukhin, A. V. Kavokin, *Sci. Rep.* **2019**, *9*, 338.

[214] J. Du, S. Liu, Z. Lin, J. Zi, S. T. Chui, *Phys. Rev. A* **2009**, *79*, 23.

[215] R. Quidant, J. C. Weeber, A. Dereux, D. Peyrade, C. Girard, Y. Chen, *Phys. Rev. E* **2002**, *65*, 036616.

[216] K. Y. Lee, C. N. Chen, Y. J. Lin, *Opt. Quantum Electron.* **2008**, *40*, 633.

[217] R. Zhao, T. Zhai, Z. Wang, D. Liu, *J. Light. Technol.* **2009**, *27*, 4544.

[218] S. M. Kamali, E. Arbabi, A. Arbabi, A. Faraon, *Nanophotonics* **2018**, *7*, 1041.

[219] P. Gutruf, C. Zou, W. Withayachumnankul, M. Bhaskaran, S. Sriram, C. Fumeaux, *ACS Nano* **2016**, *10*, 133.

[220] Y. Hu, X. Wang, X. Luo, X. Ou, L. Li, Y. Chen, P. Yang, S. Wang, H. Duan, *Nanophotonics* **2020**, *9*, 3755.

[221] D. L. Markovich, P. Ginzburg, A. K. Samusev, P. A. Belov, A. V. Zayats, *Opt. Express* **2014**, *22*, 10693.

[222] A. E. Miroshnichenko, A. B. Evlyukhin, Y. S. Kivshar, B. N. Chichkov, *ACS Photonics* **2015**, *2*, 1423.

[223] M. Odit, P. Kapitanova, P. Belov, R. Alaee, C. Rockstuhl, Y. S. Kivshar, *Appl. Phys. Lett.* **2016**, *108*, 221903.

[224] H. Wang, J. Wen, W. Wang, N. Xu, P. Liu, J. Yan, H. Chen, S. Deng, *ACS Nano* **2019**, *13*,

1739.

[225] M. W. Knight, Y. Wu, J. B. Lassiter, P. Nordlander, N. J. Halas, *Nano Lett.* **2009**, *9*, 2188.

[226] R. Xu, X. D. Wang, W. Liu, X. N. Xu, Y. Q. Li, A. Ji, F. H. Yang, J. M. Li, *Chinese Phys. B* **2012**, *21*, 025202.

[227] K. R. Catchpole, A. Polman, *Appl. Phys. Lett.* **2008**, *93*, 2008.

[228] H. A. Atwater, A. Polman, *Nat. Mater.* **2010**, *9*, 865.

[229] E. Xifré-Pérez, L. Shi, U. Tuzer, R. Fenollosa, F. Ramiro-Manzano, R. Quidant, F. Meseguer, *ACS Nano* **2013**, *7*, 664.

[230] T. Hutter, F. M. Huang, S. R. Elliott, S. Mahajan, *J. Phys. Chem. C* **2013**, *117*, 7784.

[231] N. Li, H. Wang, Y. Lai, H. Chen, J. Wang, *Part. Part. Syst. Charact.* **2020**, *37*, 2000106.

[232] L. Li, T. Hutter, A. S. Finnemore, F. M. Huang, J. J. Baumberg, S. R. Elliott, U. Steiner, S. Mahajan, *Nano Lett.* **2012**, *12*, 4242.

[233] H. Sugimoto, M. Fujii, *ACS Photonics* **2018**, *5*, 1986.

[234] Y. Wu, J. Xu, E. T. Poh, L. Liang, H. Liu, J. K. W. Yang, C. W. Qiu, R. A. L. Vallée, X. Liu, *Nat. Nanotechnol.* **2019**, *14*, 1110.

[235] A. G. Curto, T. H. Taminiau, G. Volpe, M. P. Kreuzer, R. Quidant, N. F. Van Hulst, *Nat. Commun.* **2013**, *4*, 1750.

[236] S. Bidault, M. Mivelle, N. Bonod, *J. Appl. Phys.* **2019**, *126*, 094104.

[237] A. Imamoglu, R. J. Ram, S. Pau, Y. Yamamoto, *Phys. Rev. A* **1996**, *53*, 4250.

[238] T. Volz, A. Reinhard, M. Winger, A. Badolato, K. J. Hennessy, E. L. Hu, A. Imamoğlu, *Nat. Photonics* **2012**, *6*, 605.

[239] D. Sanvitto, S. Kéna-Cohen, *Nat. Mater.* **2016**, *15*, 1061.

[240] M. Wu, S. T. Ha, S. Shendre, E. G. Durmusoglu, W. K. Koh, D. R. Abujetas, J. A. Sánchez-Gil, R. Paniagua-Domínguez, H. V. Demir, A. I. Kuznetsov, *Nano Lett.* **2020**, *20*, 6005.

[241] E. Cao, W. Lin, M. Sun, W. Liang, Y. Song, *Nanophotonics* **2018**, *7*, 145.

[242] S. Lepeshov, M. Wang, A. Krasnok, O. Kotov, T. Zhang, H. Liu, T. Jiang, B. Korgel, M. Terrones, Y. Zheng, A. Alú, *ACS Appl. Mater. Interfaces* **2018**, *10*, 16690.

[243] F. Todisco, R. Malureanu, C. Wolff, P. A. D. Gonçalves, A. S. Roberts, N. Asger Mortensen, C. Tserkezis, *Nanophotonics* **2020**, *9*, 803.

[244] J. Yan, C. Ma, P. Liu, C. Wang, G. Yang, *Light Sci. Appl.* **2017**, *6*, 16197.

[245] R. Regmi, J. Berthelot, P. M. Winkler, M. Mivelle, J. Proust, F. Bedu, I. Ozerov, T. Begou, J. Lumeau, H. Rigneault, M. F. García-Parajó, S. Bidault, J. Wenger, N. Bonod, *Nano Lett.* **2016**, *16*, 5143.

[246] M. Caldarola, P. Albella, E. Cortés, M. Rahmani, T. Roschuk, G. Grinblat, R. F. Oulton, A. V.

Bragas, S. A. Maier, *Nat. Commun.* **2015**, *6*, 7915.

[247] S. V. Makarov, I. S. Sinev, V. A. Milichko, F. E. Komissarenko, D. A. Zuev, E. V. Ushakova, I. S. Mukhin, Y. F. Yu, A. I. Kuznetsov, P. A. Belov, I. V. Iorsh, A. N. Poddubny, A. K. Samusev, Y. S. Kivshar, *Nano Lett.* **2018**, *18*, 535.

[248] M. R. Shcherbakov, A. S. Shorokhov, D. N. Neshev, B. Hopkins, I. Staude, E. V. Melik-Gaykazyan, A. A. Ezhov, A. E. Miroshnichenko, I. Brener, A. A. Fedyanin, Y. S. Kivshar, *ACS Photonics* **2015**, *2*, 578.

[249] B. Sain, C. Meier, T. Zentgraf, *Adv. Photonics* **2019**, *1*, 024002.

[250] W. K. Burns, N. Bloembergen, *Phys. Rev. B* **1971**, *4*, 3437.

[251] M. R. Shcherbakov, D. N. Neshev, B. Hopkins, A. S. Shorokhov, I. Staude, E. V. Melik-Gaykazyan, M. Decker, A. A. Ezhov, A. E. Miroshnichenko, I. Brener, A. A. Fedyanin, Y. S. Kivshar, *Nano Lett.* **2015**, *14*, 6488.

[252] A. S. Shorokhov, E. V. Melik-Gaykazyan, D. A. Smirnova, B. Hopkins, K. E. Chong, D. Y. Choi, M. R. Shcherbakov, A. E. Miroshnichenko, D. N. Neshev, A. A. Fedyanin, Y. S. Kivshar, *Nano Lett.* **2016**, *16*, 4857.

[253] K. I. Okhlopkov, P. A. Shafirin, A. A. Ezhov, N. A. Orlikovsky, M. R. Shcherbakov, A. A. Fedyanin, *ACS Photonics* **2019**, *6*, 189.

[254] G. Grinblat, Y. Li, M. P. Nielsen, R. F. Oulton, S. A. Maier, *Nano Lett.* **2016**, *16*, 4635.

[255] G. Grinblat, Y. Li, M. P. Nielsen, R. F. Oulton, S. A. Maier, *ACS Nano* **2017**, *11*, 953.

[256] M. K. Kroychuk, A. S. Shorokhov, D. F. Yagudin, D. A. Shilkin, D. A. Smirnova, I. Volkovskaya, M. R. Shcherbakov, G. Shvets, A. A. Fedyanin, *Nano Lett.* **2020**, *20*, 3471.

[257] S. V. Makarov, M. I. Petrov, U. Zywietz, V. Milichko, D. Zuev, N. Lopanitsyna, A. Kuksin, I. Mukhin, G. Zograf, E. Ubyivovk, D. A. Smirnova, S. Starikov, B. N. Chichkov, Y. S. Kivshar, *Nano Lett.* **2017**, *17*, 3047.

[258] R. Camacho-Morales, M. Rahmani, S. Kruk, L. Wang, L. Xu, D. A. Smirnova, A. S. Solntsev, A. Miroshnichenko, H. H. Tan, F. Karouta, S. Naureen, K. Vora, L. Carletti, C. De Angelis, C. Jagadish, Y. S. Kivshar, D. N. Neshev, *Nano Lett.* **2016**, *16*, 7191.

[259] L. Xu, G. Saerens, M. Timofeeva, D. A. Smirnova, I. Volkovskaya, M. Lysevych, R. Camacho-Morales, M. Cai, K. Zangeneh Kamali, L. Huang, F. Karouta, H. H. Tan, C. Jagadish, A. E. Miroshnichenko, R. Grange, D. N. Neshev, M. Rahmani, *ACS Nano* **2020**, *14*, 1379.

[260] J. Xiang, S. Jiang, J. Chen, J. Li, Q. Dai, C. Zhang, Y. Xu, S. Tie, S. Lan, *Nano Lett.* **2017**, *17*, 4853.

[261] C. Zhang, Y. Xu, J. Liu, J. Li, J. Xiang, H. Li, J. Li, Q. Dai, S. Lan, A. E. Miroshnichenko, *Nat. Commun.* **2018**, *9*, 2964.

[262] L. Sortino, P. G. Zotev, S. Mignuzzi, J. Cambiasso, D. Schmidt, A. Genco, M. Aßmann, M. Bayer, S. A. Maier, R. Sapienza, A. I. Tartakovskii, *Nat. Commun.* **2019**, *10*, 5119.

[263] G. Yang, Y. Niu, H. Wei, B. Bai, H. B. Sun, *Nanophotonics* **2019**, *8*, 2313.

[264] A. Vaskin, S. Mashhadi, M. Steinert, K. E. Chong, D. Keene, S. Nanz, A. Abass, E. Rusak, D. Y. Choi, I. Fernandez-Corbaton, T. Pertsch, C. Rockstuhl, M. A. Noginov, Y. S. Kivshar, D. N. Neshev, N. Noginova, I. Staude, *Nano Lett.* **2019**, *19*, 1015.

[265] M. Sanz-Paz, C. Ernandes, J. U. Esparza, G. W. Burr, N. F. Van Hulst, A. Maitre, L. Aigouy, T. Gacoin, N. Bonod, M. F. Garcia-Parajo, S. Bidault, M. Mivelle, *Nano Lett.* **2018**, *18*, 3481.

[266] X. Cheng, X. Zhuo, R. Jiang, Z. G. Wang, J. Wang, H. Q. Lin, *Adv. Opt. Mater.* **2021**, 2002212.

[267] C. M. Soukoulis, M. Wegener, *Nat. Photonics* **2011**, *5*, 523.

[268] W. Fan, B. Yan, Z. Wang, L. Wu, *Sci. Adv.* **2016**, *2*, 40.

[269] G. Zhang, C. Lan, H. Bian, R. Gao, J. Zhou, *Opt. Express* **2017**, *25*, 22038.

[270] Y. Nagasaki, M. Suzuki, J. Takahara, *Nano Lett.* **2017**, *17*, 7500.

[271] J. Takahara, S. Yamagishi, H. Taki, A. Morimoto, T. Kobayashi, *Opt. Lett.* **1997**, *22*, 475.

[272] K. V. Nerkararyan, *Phys. Lett. Sect. A* **1997**, *237*, 103.

[273] J. J. Burke, G. I. Stegeman, T. Tamir, *Phys. Rev. B* **1986**, *33*, 5186.

[274] E. Verhagen, A. Polman, L. Kuipers, *Opt. Express* **2008**, *16*, 45.

[275] H. Yang, R. Trouillon, G. Huszka, M. A. M. Gijs, *Nano Lett.* **2016**, *16*, 4862.

[276] Y. Liang, H. Liu, F. Wang, H. Meng, J. Guo, J. Li, Z. Wei, *Nanomaterials* **2018**, *8*, 288.

[277] A. Miroshnichenko, *Nat. Nanotechnol.* **2019**, *14*, 198.

[278] R. Quidant, R. Quidant, A. V Zayats, I. I. Smolyaninov, J. Mao, S. Blair, *Europhys. Lett. Eur.* **2002**, *60*, 663.

[279] A. Ahmadi, H. Mosallaei, *Phys. Rev. B* **2008**, *77*, 045104.

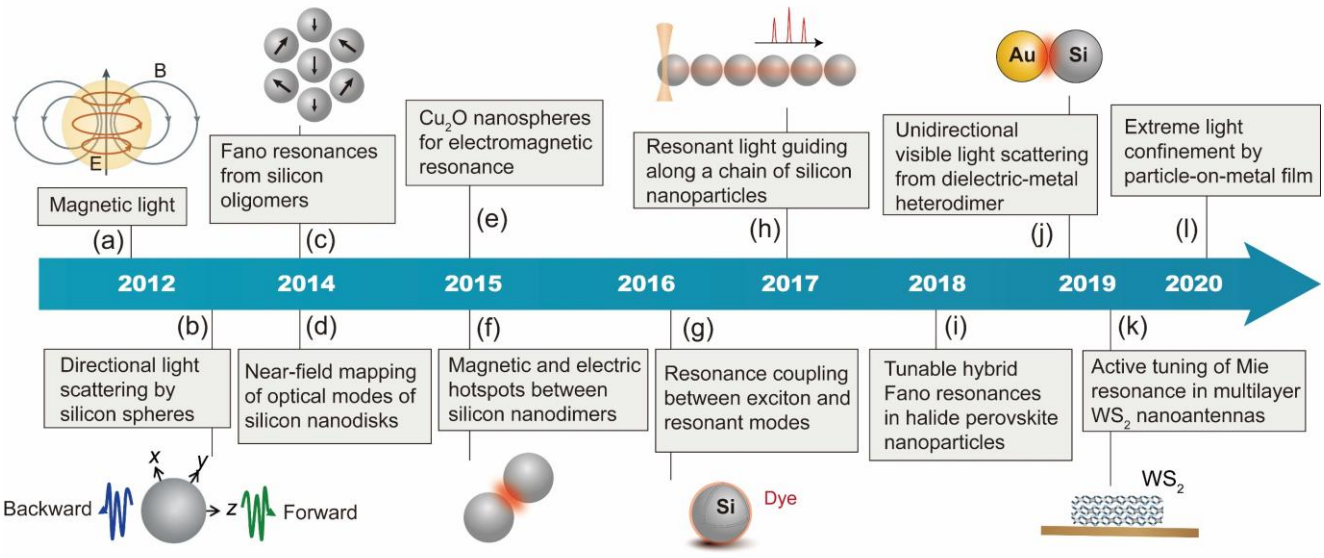

Figure 1. Selective experimental breakthroughs for the resonant scattering manipulation of dielectric nanoparticles in the visible to NIR spectral ranges. a) The first demonstration of the scattered "magnetic light" in the visible spectral range by spherical Si nanoparticles.[26] b) Directional light scattering by spherical Si nanoparticles experimentally demonstrated for the first time.[36] c) The first observation of Fano resonances in Si oligomers by Chong et al.[39] d) The near-field amplitudes and phases of localized optical modes in high-index all-dielectric nanoparticles measured by apertureless

near-field optical microscopy.[40] e) Directional forward scattering induced by the spectral overlap of the electric and magnetic dipole resonances in colloidal Cu_2O nanospheres.[41] f) Hotspots of the magnetic field in a Si dimer observed by near-field scanning optical microscopy for the first time.[42] g) The resonance coupling in heterostructures composed of Si nanoparticle core coated with J-aggregate shell.[44] h) Subwavelength confined waveguiding experimentally demonstrated by a chain of Si nanoparticles with photon energy propagation at distances beyond 500 μm.[43] i) The observation of broadly tunable Fano resonances in halide perovskite nanoparticles.[45] j) The directional scattering of a heterodimer composed of Si and Au nanospheres synthesized by a solution process.[46] k) Strong coupling between geometrical optical modes and excitons in WS_2 nanodisks demonstrated by Verre et al.[37] l) A hybrid device composed of dielectric nanodisks located on an Au surface supporting the large field enhancement.[38]

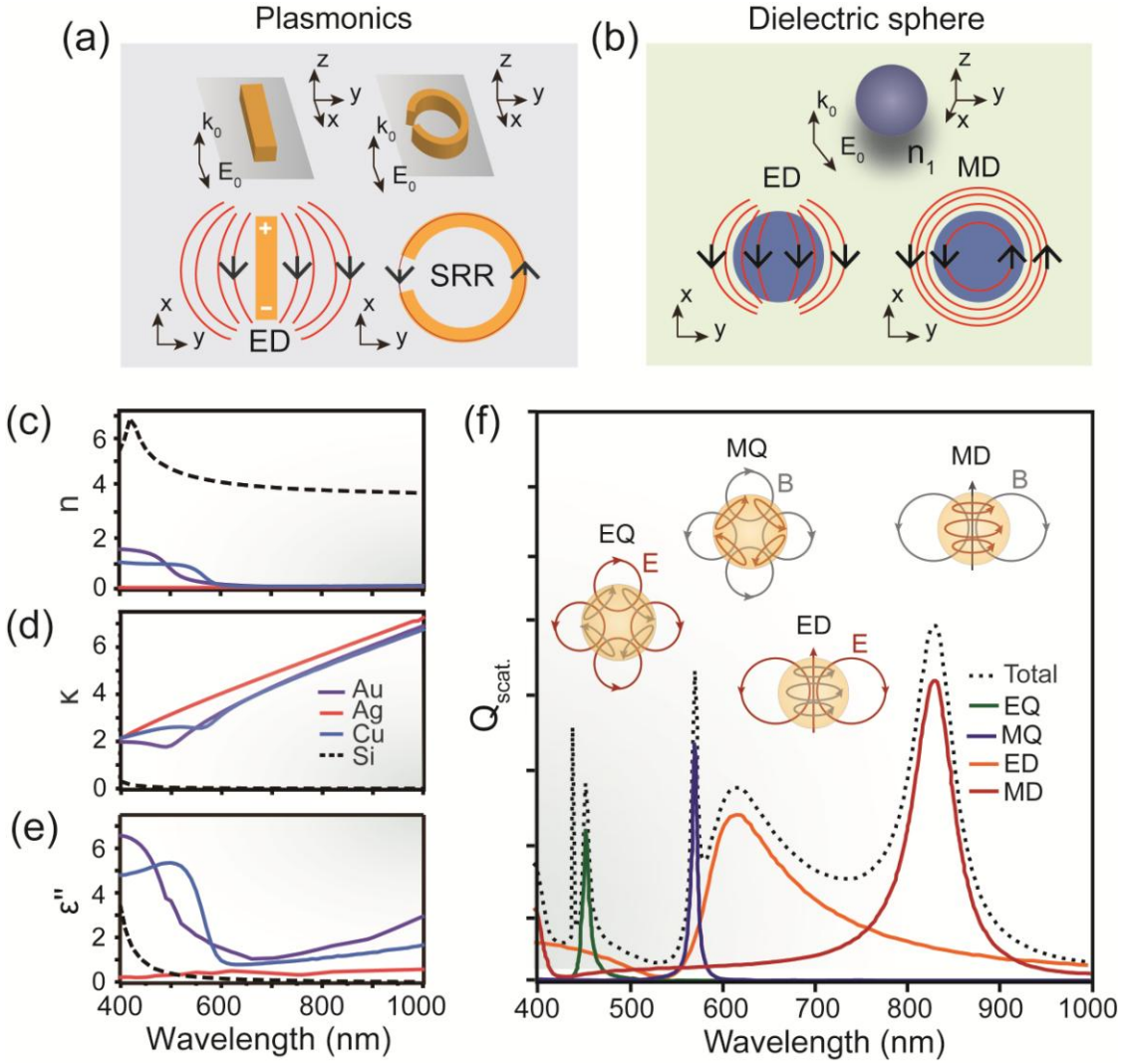

Figure 2. a) Schematic of the comparison of electric field distributions in a metallic nanorod or a split-ring resonator. b) Schematic illustration of the electric and magnetic field distributions inside a high-

refractive-index dielectric nanoparticle. c,d,e) The refractive index (n), the extinction coefficient ($\boldsymbol{K}$) and the imaginary permittivity coefficient ($\boldsymbol{\varepsilon_r''}$) against wavelength in the visible and NIR ranges. Gold (Au), silver (Ag), and copper (Cu) are represented by solid lines, while Si, the most commonly used dielectric antenna material, is represented by dashed lines. f) Decomposition of the total scattering efficiency of a single, 100-nm-diameter, high-refractive-index (n = 4) nanosphere into the contributions of various Mie coefficients a_1 (essentially an electric dipole, ED), b_1 (an essentially a magnetic dipole MD), a_2 (essentially an electric quadrupole, EQ) and b_2 (essentially a magnetic quadrupole, MQ). The insets show the simplified electric and magnetic field profiles of the different resonant modes. (a,b) Reproduced with permission.[5] Copyright 2017, Optical Society of America.

Table 1 | Typical examples of individual dielectric nanoparticles

Refractive index (n)	Nanostructures	Method of fabrication	Spectral region (nm)	Main optical features	Refs.
HRID (n ≥ 3.0)	Si nanosphere	Femtosecond laser ablation	400 – 1000	Directional scattering	[36]
				Magnetic dipole resonance	[25,26]
				Optical printing	[119]
		Laser printing	400 – 800	Multicolor scattering	[118,120]
		Chemical vapor deposition	600 – 1500	Magnetic response	[28,121]
		Dewetting-based process	400 – 1000	Multicolor scattering	[115]
	Si nanowire	Chemical vapor deposition	400 – 1000	Multicolor scattering	[23,113]
		Electron beam lithography		Magnetic resonance	[112]
	Si nanoring		600 – 1000	High-order multipole scattering	[175]
	Si hollow nanocylinder		400 – 700	Multicolor scattering	[174]
	GaAs sphere	Laser printing	600 – 1000	Zero optical backscattering	[125]
	PbTe nanosphere	Laser ablation	≥ 4 μm	Thermo-optic tuning	[128]
	$Ge_2Sb_2Te_5$	Electron beam lithography	2.5 – 6 μm	Active control of anapole states	[129]
	WS_2 nanodisks	Exfoliation followed by electron beam lithography	700 – 900	Mie mode-exciton polariton interaction	[37]
MRID (1.7 ≤ n ≤ 3.0)	Cu_2O nanosphere	Wet-chemistry method	400 – 900	Magnetic response and directional scattering	[41,140]
	TiO_2		300 – 900	Multicolor scattering	[137,159]

	nanoparticle				
	$CsPbBr_3$ nanocube	Two step deposition technique	500 – 1000	Scattering and nanolaser	[151]
	$MAPbBr_3$ nanoparticle	Deposition technique followed by laser ablation	400 – 800	Tunable Fano resonance	[45]
	$BaTiO_3$ nanoparticles	Solvothermal	450 – 600	Visible-light second-harmonic generation	[147,148]
	$LiNbO_3$ nanocubes	Solvothermal	350 – 450	Near-UV second-harmonic generation	[146]
	ZnS nanospheres	Precipitation	350 – 900	Color filtering	[130]
LRID ($0 \leq n \leq 1.7$)	Metal-dressed SiO_2 nanosphere	Two-step metal deposition process	400 – 800	Mie resonance of low-refractive-index nanoparticles	[154]
	Polymer sphere assemblies	Polymer sphere assemblies	300 – 1000	Photonic band gap and resonant Mie scattering	[160]

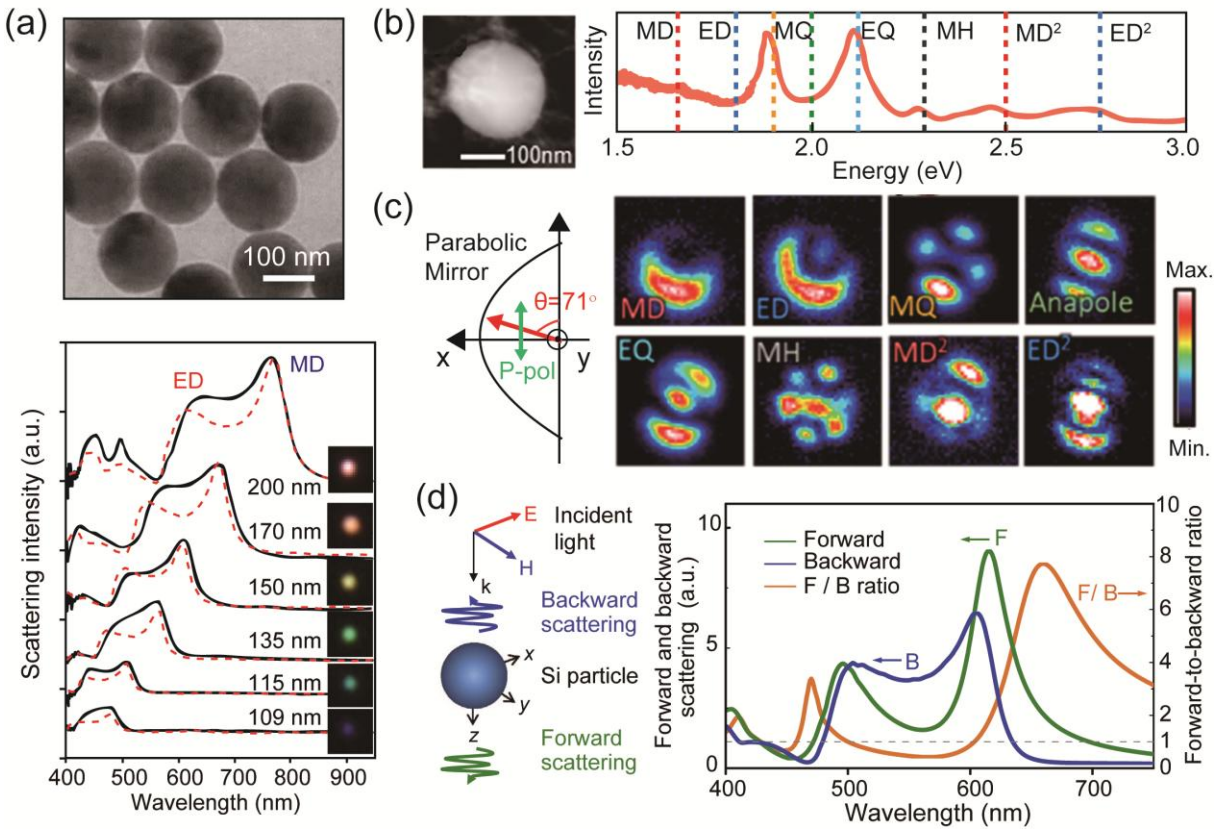

Figure 3. a) (Top) Transmission electron microscopy (TEM) image of monodisperse Si nanospheres with an average diameter of 162 nm. (Bottom) Measured (black lines)/calculated (red dashed lines) scattering spectra and their corresponding dark-field images of single Si nanospheres with different diameters. Their dark-field images are also shown as insets and the diameters of the used Si nanospheres are indicated. b) Scanning transmission electron microscopy dark-field image of a single Si nanosphere with a diameter of 200 nm and its corresponding cathodoluminescence spectrum. The peaks at representative energies are labeled with their corresponding electric and magnetic resonance modes. From low to high in terms of energy, these modes are the magnetic dipole (MD), electric dipole (ED), magnetic quadrupole (MQ), electric quadrupole (EQ), magnetic hexapole (MH), second-order magnetic dipole (MD^2), and second-order electric dipole (ED^2) modes. c) (Left) Schematic illustration of the detection configuration. The green arrow represents the polarization direction, and the red arrow denotes the detection direction. (Right) Photon maps of the representative resonant modes mentioned in b. d) (Left) Mie modeling scheme: the single Si nanosphere is excited by a plane wave, whereas the scattered light is divided into forward and backward scatterings. (Right) Calculated scattering spectra of a single Si nanosphere with a diameter of 150 nm in free space. The blue and green curves correspond to the backward and forward scattering cross-sections, respectively, whereas the orange curve denotes the forward-to-backward ratio. (a) Reproduced with permission.[27]

Copyright 2020, Wiley-VCH; (b,c) Reproduced with permission.[124] Copyright 2019, American Chemical Society; (d) Reproduced with permission.[36] Copyright 2013, Springer Nature.

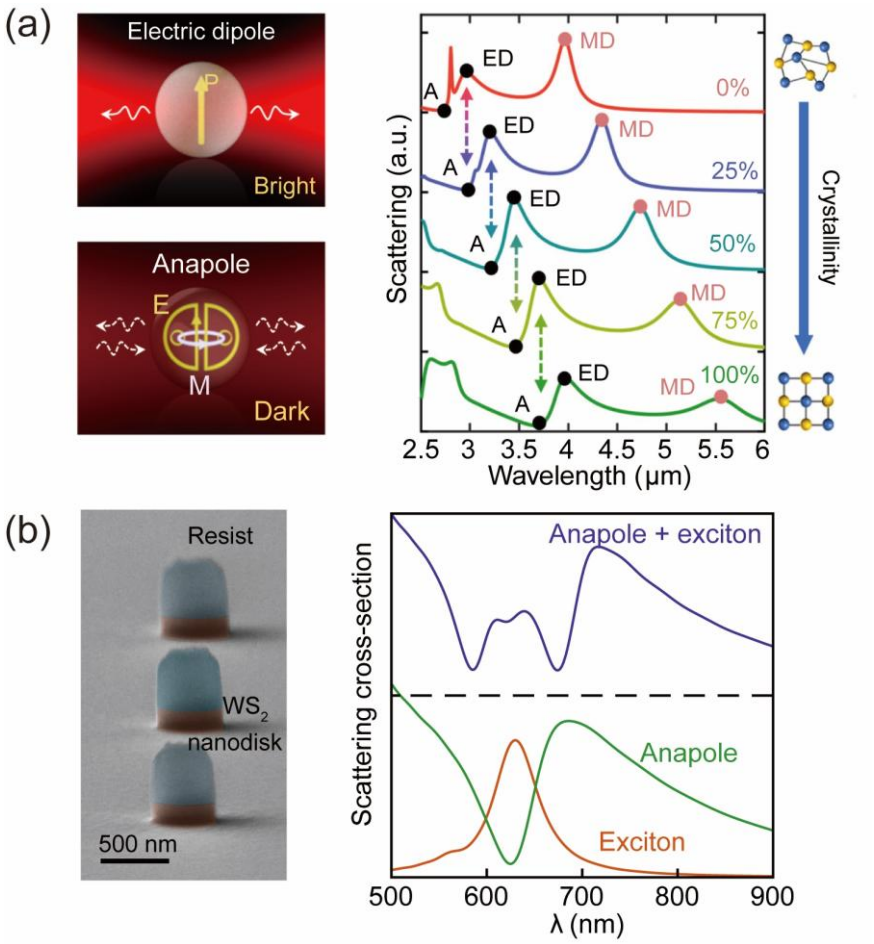

Figure 4. a) (Left) Schematic of the scattering bright (ED) and dark (Anapole) states in a GST sphere. (Right) Simulated scattering spectra of a GST sphere (R = 450 nm) with different crystallinities. With increasing donation of anapole states (marked as A), the resonance originating from both ED and MD modes shifts continuously to the red spectrum. b) (Left) Side-view scanning electron microscope (SEM) image of WS_2 nanodisks with false-color. (Right) Simulated scattering cross-section spectra of a WS_2 nanodisk (R = 130 nm and H = 55 nm) in a vacuum with cessation of exciton resonance (green) or high-refractive-index background (red) and with actual permittivity resulting from exciton coupling and a high background index (purple). (a) Reproduced with permission.[129] Copyright 2019, Springer Nature; (b) Reproduced with permission.[37] Copyright 2019, Springer Nature.

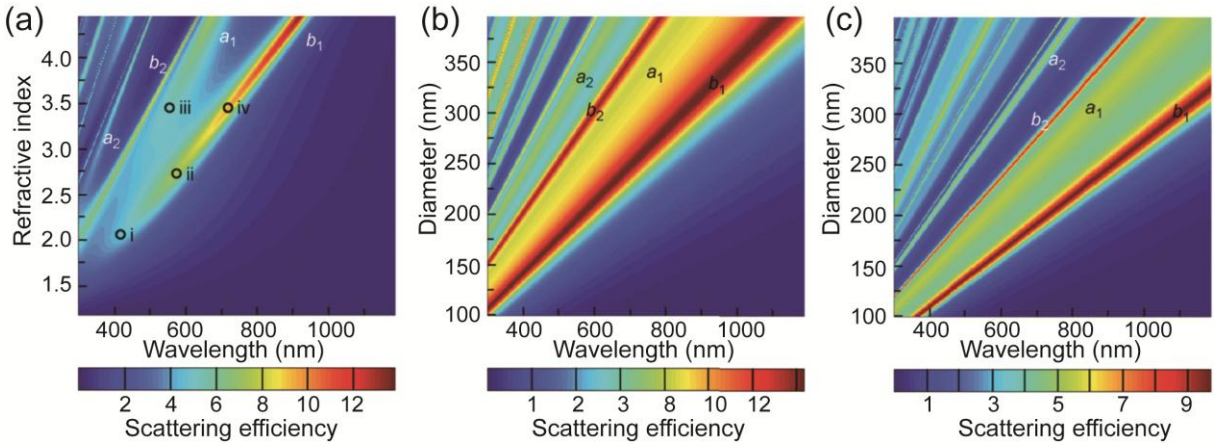

Figure 5. a) Scattering efficiency as a function of wavelength and refractive index of a 200-nm-diameter dielectric nanosphere. b,c) Scattering efficiency as a function of wavelength and particle size for a dielectric nanosphere with refractive indices of 2.7 and 3.5. When the refractive index is smaller than ≈1.7, there is no resonant response from the dielectric nanospheres in the visible region. When the RI is increased from ≈1.7 to ≈3.0, electric and magnetic dipole resonances start to appear and become gradually stronger, while still spectrally close to each other. Once the RI is larger than ≈3.0, the dipole resonance tends to spectrally separate from each other and the high-order resonance such as electric and magnetic quadrupole modes become apparent in the visible region. (a,b,c) Reproduced with permission.[41] Copyright 2015, Wiley-VCH.

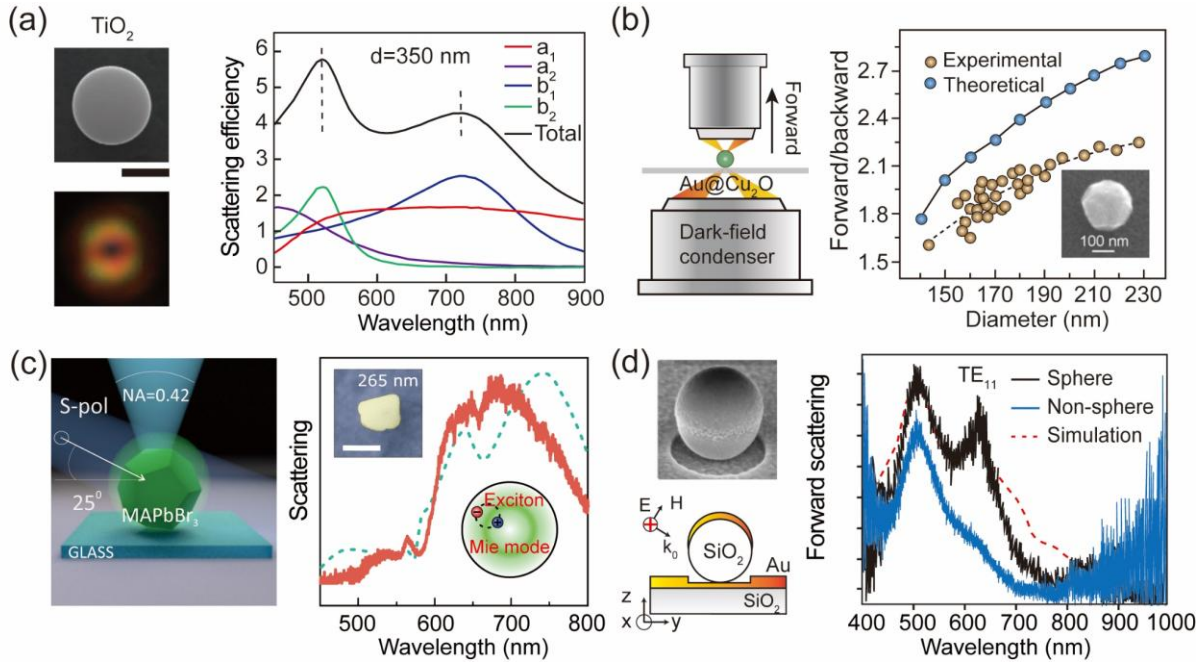

Figure 6. a) (Left) SEM and corresponding dark-field scattering image of a single TiO_2 nanosphere. The scale bar is 500 nm. (Right) Calculated scattering spectrum of the nanosphere with a diameter of 350 nm and a refractive index of 2.0. The total spectrum is degenerated into electric and magnetic resonance modes of different orders. b) (Left) Schematic illustration of the forward scattering measurements. (Right) Evolution of the ratio between forward and backward scattering at the resonance peak as a function of the $Au@Cu_2O$ nanosphere diameter. c) (Left) Scheme of the dark-field scattering spectroscopy of single $MAPbBr_3$ nanoparticles. (Right) Measured dark-field(solid) and simulated (dashed) spectra of $MAPbBr_3$ nanoparticles (265 nm). The inset shows the SEM image of a $MAPbBr_3$ nanoparticle with a scale bar of 200 nm. d) (Left) SEM image and schematic pattern of a metal dressed SiO_2 nanosphere. (Right) Measured forward (black) and simulated (red) scattering spectra of a 486-nm-diameter nanosphere together with a test area deprived of a nanosphere (blue). (a) Reproduced with permission.[137] Copyright 2015, Wiley-VCH; (b) Reproduced with permission.[41] Copyright 2015, Wiley-VCH; (c) Reproduced with permission.[45] Copyright 2018, American Chemical Society; (d) Reproduced with permission.[154] Copyright 2018, American Physical Society.

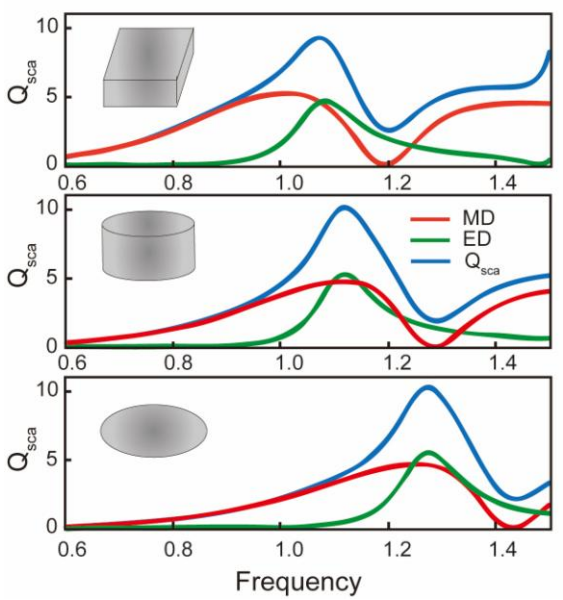

Figure 7. A collection of scattering efficiency curves for parallelepiped (top panel), cylindrical (middle panel), and spheroid (bottom panel) particles with the same aspect ratio of 2.086 and refractive index of 3.5. Reproduced with permission.[166] Copyright 2015, American Chemical Society.

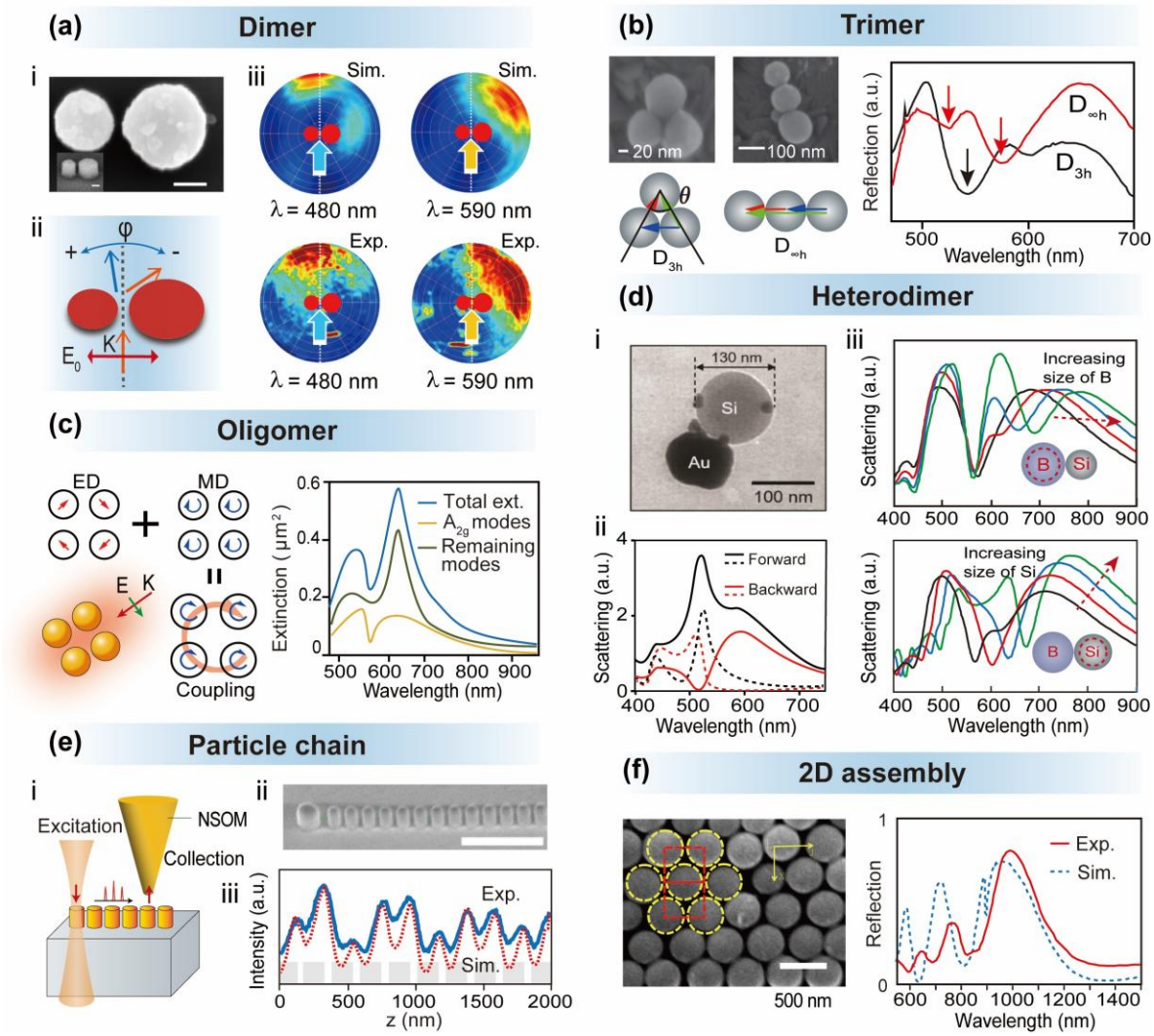

Figure 8. a) i) SEM image of the asymmetrical dimer of Si nanodisks. The scale bar is 100 nm. ii) Scheme of the directional scattering from the asymmetrical dimers. K and E represent the incident and polarization directions of the electromagnetic wave, whereas φ is the peak scattering angle. iii) Numerical and experimental scattering patterns of the asymmetrical dimer which are monitored under the incident light at λ = 480 nm and λ = 590 nm. b) (Left) SEM images and corresponding schematic diagrams of the trimers with different aggregation states depending on the vertex angle θ. When θ = 60, the trimer belongs to the D_{3h} symmetry group. When θ = 180, the trimer belongs to the $D_{\infty h}$ symmetry group. (Right) The measured dark-field reflection spectra of D_{3h} (black curve) and $D_{\infty h}$ (red curve) trimers. The three arrows represent the dips caused by nanosphere interactions. c) (Left) Schematic of a symmetrical nanosphere quadrumer excited by an in-plane s-polarized plane wave. The basis vectors for the optical response of the tetramer electric and magnetic dipoles are represented by the red and blue arrows, respectively, and referred to A_{2g} (magnetic-like) eigenmodes. A collective optically induced magnetic resonance of the entire structure is sustained by the collective circulation of the electric response of the individual nanosphere. (Right) Simulated extinction spectrum (blue curve) and corresponding electromagnetic eigenmode decomposition of the Si tetramer. The yellow

and green curves show the respective contribution of A_{2g} eigenmodes and the remaining modes to the overall extinction. d) (i) TEM image of an Si–Au heterodimer. (ii) Calculated forward (black) and backward (red) scattering spectra of an Si nanosphere (dashed lines) and an Si–Au heterodimer (solid lines). (iii) Experimentally measured backward scattering spectra of the B-Si dimers with different diameters. The top one shows spectral fine-tuning by changing the diameter of B nanospheres, whereas the bottom one shows spectral coarse tuning by changing the diameter of Si nanospheres. e) (i) Schematic of the measurement setup showing the excitation of the waveguide with linearly polarized light focused on the origin and collection of evanescent fields with an uncoated near-field scanning optical microscopy (NSOM) tip. (ii) SEM image of the particle chain of Si nanodisks. The scale bar is 500 nm. (iii) Experimental cross-section of the NSOM data illustrating the intensity of 10-unit cells. f) (Left) SEM image of a 2D-Si photonic crystal. The scale bar is 500 nm. (Right) Reflection spectra obtained from both the experiment (red solid curve) and FDTD simulation (blue dashed curve) of the 2D structure. (a) Reproduced with permission.[202] Copyright 2017, American Chemical Society; (b) Reproduced with permission.[184] Copyright 2015, Springer Nature; (c) Reproduced with permission.[207] Copyright 2015, American Chemical Society; (d) (Left) Reproduced with permission.[46] Copyright 2019, Wiley-VCH; (Right) Reproduced with permission.[211] Copyright 2016, American Chemical Society; (e) Reproduced with permission.[43] Copyright 2017, American Chemical Society; (f) Reproduced with permission.[121] Copyright 2013, Springer Nature.

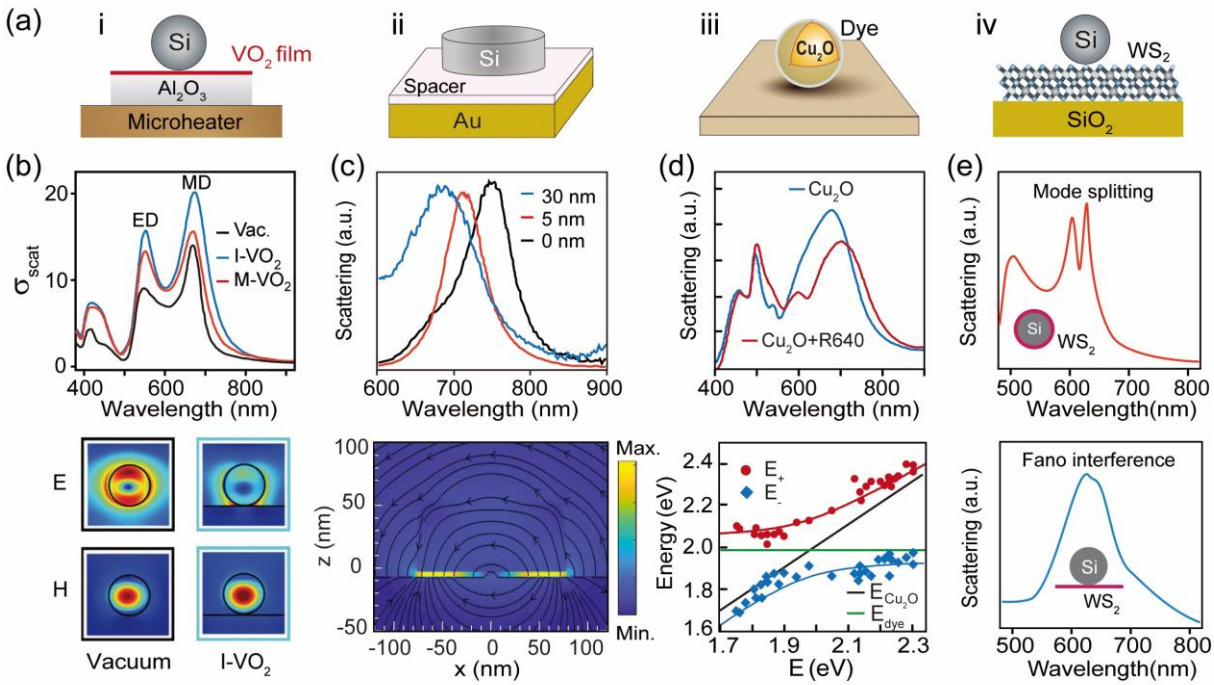

Figure 9. a) Schematic of couplings of an Si particle to a VO_2 film (i), an Si disk to a metal film (ii), a Cu_2O sphere to dye molecules (iii), and an Si particle to 2D materials (iv). b) Theoretical scattering spectra (top) and corresponding electric and magnetic field amplitudes (bottom) at the magnetic dipole resonance of a single Si nanosphere (d = 170 nm) in a vacuum or on various VO_2 films. c) (Top) Normalized experimental dark-field scattering spectra of Si nanodisk-Au mirror hybrid nanostructures with different spacer thickness values. (Bottom) The near-field distribution was recorded at the resonance wavelength of the Si nanodisk coupled to the metal film, in the incidence plane and around the gap. d) (Top) Dark-field scattering spectra of a pristine Cu_2O nanosphere and a Cu_2O nanosphere coated with R640 aggregates. (Bottom) Plot for the hybrid mode energies at scattering peaks as a function of the resonance energies of the Cu_2O nanospheres. E^+ and E^- represent the energies of the high- and low-energy scattering peaks of the Cu_2O nanosphere coated with R640. The energies of the pristine Cu_2O nanospheres and R640 aggregates are also drawn as diagonal and horizontal lines, respectively. e) Theoretical scattering spectra of an Si nanosphere coated with a monolayer of WS_2 (top) and one deposited onto a monolayer of WS_2 (bottom). (b) Reproduced with permission.[190] Copyright 2019, The Royal Society of Chemistry; (c) Reproduced with permission.[38] Copyright 2020, Wiley-VCH; (d) Reproduced with permission.[193] Copyright 2018, American Chemical Society; (e) Reproduced with permission.[224] Copyright 2019, American Chemical Society.

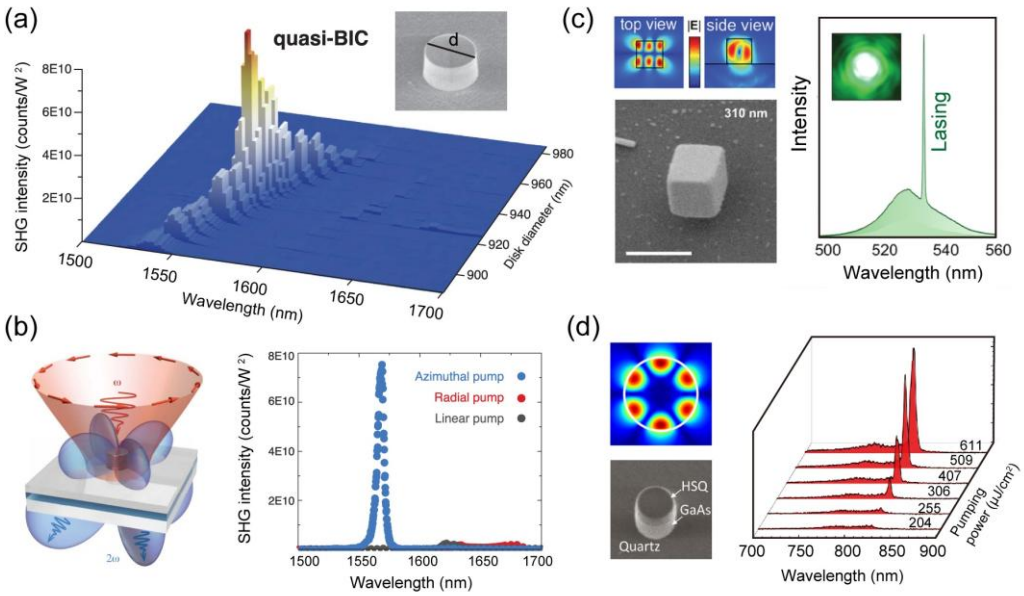

Figure 10. (a) 3D emission intensity mapping of second harmonic signals measured as a function of the excitation wavelength and particle diameter. The inset shows the SEM image of an individual AlGaAs nanoresonator with the diameter *d* of ~930 nm; (b) Schematic of SHG in a AlGaAs nanoresonator under azimuthally polarized vector beam excitation (left) and measured second harmonic intensity as a function of the pump wavelength (right); (c) Simulated near-field electric field patterns of perovskite nanocube (upper left) and the SEM image of the corresponding perovskite nanocube (left bottom). Scale bar is 500 nm. Lasing action of the perovskite nanocube empowered by low-order Mie-resonant modes (right). (d) Simulated near fields of the supercavity mode in the XY planes of the cylinder (upper left) and the SEM image of an individual GaAs nanocylinder with diameter of 500 and height of 330 nm (left bottom). Lasing action of the GaAs nanocylinder at different pumping flux (right). (a,b) Reproduced with permission.[9] Copyright 2020, AAAS; (c) Reproduced with permission.[151] Copyright 2020, American Chemical Society; (d) Reproduced with permission.[13] Copyright 2020, American Chemical Society.

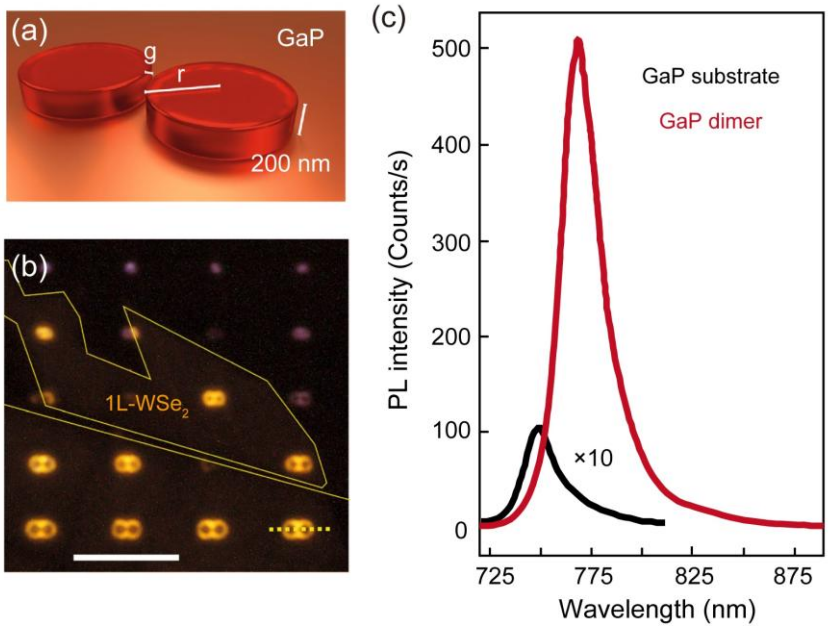

Figure 11. (a) Diagram of a GaP dimer nanoresonator with a height of 200 nm, gap spacing of *g*, and pillar radius of *r*. (b) Optical microscopic image of dimer nanoresonators array covered with atomically thin WSe_2. Scale bar is 10 μm. (c) Photoluminescence spectra for monolayer WSe_2 placed on top of dimer GaP nanoresonators and on the planar GaP. (a,b,c) Reproduced with permission.[262] Copyright 2019, Springer Nature.

Table of Contents

Subwavelength dielectric particles have emerged as a new class of photonic building blocks that enable enhanced light-matter interactions within nanometric volumes. This review highlights recent theoretical and experimental advances that have fostered the ability to shape the optical properties of dielectric nanoparticles, from resonant single-particle scattering characteristics to the multimodal interferences of complex particle dispositions.

Jiahui Xu, Yue Wu, Pinzheng Zhang, Yiming Wu, Renaud A. L. Vallée, Suli Wu* and Xiaogang Liu*

Resonant Scattering Manipulation of Dielectric Nanoparticles